Is JPEG AI going to change image forensics?

Supplementary Material

7. Neural image compression and JPEG AI specification

Neural image compression basics. In Neural Image Compression (NIC), an input image is transformed into a compact file or bitstream for storage or transmission, which is later used to reconstruct the original image. The basic approach involves mapping an image vector $\mathbf{I}$ to a latent representation $\mathbf{y}$ using a convolutional autoencoder. This latent representation is then quantized to $\hat{\mathbf{y}}$ and compressed into a bitstream using an entropy coding method such as arithmetic coding. During reconstruction, the received bits are decoded via reverse entropy coding, and the resulting $\hat{\mathbf{y}}$ is fed into a CNN decoder to produce the reconstructed image $\hat{\mathbf{I}}$. These models can be trained end-to-end with the help of differentiable proxies for entropy coding.

As pointed out in Sec. 2, many techniques exist to perform such operations. In 2017, Theis et al. [84] and Ballé et al. [19] introduced the first deep-learning approaches for image compression. [84] proposed compressive autoencoders that learn end-to-end optimized lossy image compression, aiming to outperform traditional codecs, especially at lower bitrates. [19] presented the first pipeline that jointly optimizes all components of the compression pipeline, achieving superior rate-distortion performance compared to traditional codecs. Building upon their previous work, in [20], Ballé et al. incorporate a scale hyperprior to model the entropy of the latent representations more accurately, leading to improved compression efficiency. Minnen et al. [67] combine autoregressive models with hierarchical priors to better capture spatial dependencies in images, enhancing the performance of learned image compression systems. Choi et al. [31] present a conditional autoencoder that enables variable-rate image compression within a single model, adjusting compression rates on the fly without retraining. In 2021, Yang et al. [94] proposed slimmable autoencoders that adjust their network width to accommodate different compression rates, making neural compression more adaptable and efficient. Zhu et al. [99] in 2022 presented a unified entropy model using multivariate Gaussian mixtures to better model the distribution of latent representations, improving compression efficiency.

JPEG AI scheme specification. The astonishing results from the literature pushed in 2019 the JPEG Standardization Committee to launch the first image coding specifications based on end-to-end learning [50], namely the JPEG AI initiative. At its core, JPEG AI follows a similar structure to standard neural image compression algorithms. In particular, we refer the reader to Fig. 2 [51] for the overall JPEG AI standard scheme specification. The encoder consists of a NN-based analysis transform that computes the latent information $\mathbf{y}$ of the input image $\mathbf{I}$. Next, $\mathbf{y}$ is processed by a latent domain prediction module, generating a latent residual $\hat{\mathbf{r}}$, and by a hyperprior encoder, producing a hyperprior $\hat{\mathbf{z}}$, as proposed in the foundational work by Ballé et al. [20]. For entropy decoding, a latent prediction network retrieves $\hat{\mathbf{y}}$, which is finally input into the synthesis transform at the decoder for reconstructing the image $\tilde{\mathbf{I}}$.

As explained in Sec. 2, JPEG AI enforces strict compliance requirements on manufacturers as a standardized format, limiting the customization options within the compression pipeline. Although certain architectural modifications are permitted (indicated by the red modules of Fig. 2), such as adjustments to the analysis transform, to the hyperprior encoder network, or retraining for specific content types to improve performance, these changes are restricted. The modified latent space must still function within the official JPEG AI framework to ensure compatibility [51].

8. Experimental setup additional details

Experiments reproducibility. All code and additional figures and tables for all detectors is available at the following URL https://github.com/polimi-ispl/jpeg-ai-antifor.

Synthetic image detectors. We provide some more information regarding the forensic detectors presented in Sec. 4:

- [89]: a ResNet-50 [45], pre-trained on the Imagenet dataset and then finetuned on a dataset of real and deepfake images generated through the ProGAN [53] architecture. This detector is available in two variants, i.e., [89]-A, trained with an augmentation of Gaussian blurring and JPEG compression applied to each image with a probability of 10%, and [89]-B, trained with the same augmentation pipeline but applied with a probability of 50%;
- [43]: another ResNet-50 trained with the same setup of [89], however avoiding down-sampling of the features extracted in the first layer of the network;
- [33]: same solution as [43], but in this case, the authors train the network on a dataset of Latent Diffusion [77] deepfake samples;
- [71]: a frozen Vision Transformer (ViT) [57] pre-trained on the CLIP task, to which a final classification layer is finetuned with same dataset of [89];
- [35]: a similar approach to [71], where the authors substitute the final classification layer with a Support Vector Machine (SVM). The SVM is finetuned with only 1000

real samples from the COCO datasets and 1000 deepfakes generated with Latent Diffusion. In this case, too, we have two variants of the detector, i.e., [35]-A, trained without augmentation, and [35]-B, trained with compression and resize as data augmentation;

- [64]: an EfficientNet-B4 [83] performing a patch-based analysis of the image and aggregating multiple scores to decide the "fakeness" of the sample. This detector is trained exclusively on datasets of human faces, with deepfake samples coming from various generators, including GANs, transformers, and diffusion models;
- [82]: a method focusing on detecting deepfakes by analyzing structural artifacts introduced during the upsampling operations in generative networks like GANs and diffusion models, namely Neighboring Pixel Relationships (NPR). These artifacts create local interdependencies among neighboring pixels in synthetic images. NPR captures and characterizes these relationships to identify forgeries effectively.

Synthetic image detection datasets. To test the performances of every detector in normal conditions, we include for every pristine test set a synthetic "counterpart". These images have been selected by the original authors of the detectors to depict content similar to that of the pristine ones but are generated using different image generation techniques. In total, we considered 20 different generation techniques ranging from GANs to diffusion models, namely Guided Diffusion [39], Latent Diffusion [77], Taming Transformers [42], DALL·E [76] in various versions (i.e., mini [2], 2 [6], and 3 [7]), GLIDE [70], Stable Diffusion [77] in various versions (i.e., 1.3 [12], 1.4 [13], XL [15], and 2 [14]), Adobe Firefly [8], MidJourney v5 [11], BigGAN [27], GauGAN [73], StyleGAN [54], StyleGAN2 [56], ProGAN [53], and StarGAN [30]. Tab. 6 report their relationships with the different pristine datasets used in our evaluation.

9. Synthetic image detection additional results

Preliminary analysis on synthetic detection. Tab. 7 reports the results for the simple case of synthetic image detection *without* JPEG AI image compression of the test samples. We report the complete numbers for all detectors on all datasets.

We tested each detector only on the datasets on which the original authors first proposed the method. [64] represents the only exception since the authors reported good generalization capabilities on various semantic content despite training their solution only on human faces. As the reader can quickly inspect, all detectors achieve acceptable performance, with only two cases below the 0.75 threshold for the AUC, i.e., [35]-B on LAION and [64] on COCO.

JPEG AI quality analysis. Tab. 8 reports a complete quality analysis of the pristine JPEG AI compressed samples.

Table 6. Synthetic image generation techniques used in our experiments and their relationships with pristine datasets' content.

	CelebA	COCO	FFHQ	Imagenet	LAION	LSUN	RAISE
BigGAN [27]				✓			
GauGAN [73]		✓					
ProGAN [53]						✓	
StarGAN [30]	✓						
StyleGAN [54]						✓	
StyleGAN2 [56]			✓			✓	
GLIDE [70]		✓			✓		✓
Guided Diffusion [39]				✓	✓	✓	
Latent Diffusion [77]		✓	✓	✓		✓	
Taming Transformers [42]			✓	✓			
DALL·E [2, 6, 7, 76]		✓			✓		✓
Stable Diffusion [12–15, 77]		✓					✓
Adobe Firefly [8]							✓
MidJourney v5 [11]							✓

Table 7. AUC results of the various detectors on all datasets considered for the real VS synthetic image detection task. Results below the 0.75 threshold are reported in red. Entries signed with a – indicate that the detector has not been tested on that particular dataset.

	Dataset						
Detector	LSUN	Imagenet	COCO	CelebA	FFHQ	LAION	RAISE
[89]-A	0.99	0.88	0.92	0.98	–	–	–
[89]-B	0.98	0.90	0.98	0.95	–	–	–
[43]	–	0.89	0.96	–	0.93	–	–
[33]	–	0.87	0.96	–	0.89	–	–
[71]	0.98	0.99	1.00	0.99	–	0.96	–
[35]-A	0.95	0.97	0.97	–	0.96	0.96	0.80
[35]-B	0.79	0.83	0.89	–	0.88	0.74	0.86
[82]	0.94	0.91	1.00	1.00	–	0.99	–
[64]	0.86	0.87	0.71	1.00	1.00	0.98	0.83

To achieve this, we computed the following metrics:

- Feature Similarity (FSIM) [98]: a metric based on phase congruency and gradient magnitude to assess quality. The value range for FS is between 0 and 1, with 1 indicating the highest quality;
- Multi-Scale SIMilarity index (MS-SSIM) [91]: evaluates image quality by comparing details across resolutions. Typical values range between 0 and 1, with 1 indicating the highest quality;
- Normalized Laplacian Pyramid (NLP) [58]: based on local luminance and contrast, it uses a Laplacian pyramid decomposition. We normalize the scores in a $0 - 1$ range, with 1 indicating higher quality;

- Visual Information Fidelity (VIF) [80]: measures the loss of perceived information using natural scene statistics. Values range from 0 to infinity, with higher scores indicating better quality;
- Video Multimethod Assessment Fusion (VMAF) [59]: developed by Netflix, it assesses quality by fusing scores from multiple algorithms. Scores range from 0 to 100, with high values indicating better quality.

All these metrics have been suggested in the JPEG AI Call For Evidence [1], and we computed them using the official JPEG AI Reference Software [10]. The samples present an overall high perceptual quality as the reader can quickly inspect, even at low BPP values.

Scores distributions. Fig. 7 to Fig. 13 report the scores distribution of the detectors [43], [35]-A, [71], and [82] while varying the JPEG AI compression ratio or the JPEG quality factor of the compressed images. We report one plot for each dataset on which we tested the detectors. Results are in line with the ones reported in Fig. 4 and Fig. 5 of the main paper: while increasing the JPEG AI compression ratio creates a "shift" of the scores distribution towards the right, i.e., towards "deepfake"-like scores above the 0 threshold, standard JPEG moves the distribution towards the left, i.e., towards "pristine "-like scores below the 0 threshold. Such results are particularly relevant for the [82] detector. This tool looks for NPR, i.e., the local interdependence between image pixels caused by up-sampling operators. Such a trace seems particularly sensitive to JPEG compression. Indeed, we can see in Fig. 12d and Fig. 12f how even the score distribution for pristine samples is moved below the distribution of pristine uncompressed images. However, this result should not surprise us, as it is well known in the forensic community that JPEG compression could conceal traces relative to the image history [74]. We refer the reader to the code repository to visualize more distribution score plots.

Complete analysis of JPEG AI compression ratio. Tab. 9 to Tab. 17 report the results of the experiments by varying the compression ratio of JPEG AI for each detector on every single dataset. For all tables, as commonly done in deepfake detection tasks, we evaluate the BA, FPR, and FNR at the 0 threshold.

Comparison with standard JPEG. Tab. 18 to Tab. 26 report the results of the experiments varying the quality factor of JPEG for each detector on every single dataset. For all tables, as commonly done in deepfake detection tasks, we evaluate the BA, FPR, and FNR at the 0 threshold.

Comparison with other compression formats. To evaluate if the behavior observed for JPEG AI and JPEG is specific to these two compression formats, or it could be more generally attributed to the difference between classic and neural image compression, we repeated the experiment of Sec. 5 considering two other common standards: HEIC and WebP [17]. Tab. 27 and Tab. 28 report the results for the detector [82], considering common QF values, and evaluating the BA, FPR, and FNR at the 0 threshold. For both WebP and HEIC we observe a similar trend to the JPEG experiments, i.e., a sharp increase in FNR, but not in FPR. This element further corroborates our previous finding: JPEG AI represents an unicum among image compression formats, due to its adoption of NNs, posing an unprecedented challenge to multimedia forensics practitioners.

10. Image splicing localization additional results

Fig. 14 to Fig. 17 report some examples of output maps $\tilde{\mathbf{M}}$ for the TruFor and MMFusion detectors. In all plots, the detectors process the same DSO1 input image compressed with different JPEG AI BPP.

As we reported in Sec. 5 of the main paper, decreasing the JPEG AI compression ratio degrades the quality of the maps $\tilde{\mathbf{M}}$. All detectors do not correctly identify all the manipulated pixels in the tampered with area, while flagging many pristine pixels as manipulated. Whenever the BPP values go over 1.0, the output maps tend to match more closely the ones obtained when processing samples in their original format. This is the case, for instance, of Fig. 14.

However, it is interesting to notice that, for certain samples, increasing the BPP during compression does not lead to a better $\tilde{\mathbf{M}}$. For example, the output of MMFusion in Fig. 16 maintains a high number of false positives even for BPP $= 1.0$ and BPP $= 2.0$, and TruFor shows a similar behavior in Fig. 17. Therefore, while the overall tendency highlighted in Tab. 5 is clear, these examples seem to suggest that there is no guarantee that compressing images with high BPP values will not interfere with the responses of the detectors.

11. Double JPEG AI compression

The study field relative to multiple JPEG compression is lively [74]. Therefore, in the following, we briefly analyze some of the implications of double JPEG AI compression. Please notice that this analysis is not exhaustive, and we plan to explore the more profound implications of double JPEG AI in future studies.

Synthetic image detection. Fig. 18 reports the scores of the [43] detector extracted from pristine images compressed in the scenarios illustrated in Sec. 5.3, namely i) single JPEG AI compression, ii) double JPEG AI compression where the original-format images have been first compressed with the lowest BPP considered, i.e., BPP= 0.12, and then re-compressed at various BPP values, and iii) the original-format images have been first compressed with the highest BPP considered, i.e., BPP= 2.0, and then re-compressed at various BPP values.

Fig. 18b reports the results for the first scenario. As we

Table 8. JPEG AI Call For Evidence [1] quality metrics for our dataset of JPEG AI images. For clarity's sake, we abbreviate the metrics as follows: FSIM as FS, MS-SSIM as MS, NLP as NL, VIF as VI, and VMAF as VF.

	BPP = 0.12	BPP = 0.25	BPP = 0.5	BPP = 0.75	BPP = 1.0	BPP = 2.0
Dataset	FS / MS / NL / VI / VF	FS / MS / NL / VI / VF	FS / MS / NL / VI / VF	FS / MS / NL / VI / VF	FS / MS / NL / VI / VF	FS / MS / NL / VI / VF
Imagenet	36.57/0.96/0.42/36.27/76.65	38.36/0.98/0.54/38.00/83.71	40.63/0.99/0.64/39.90/88.92	42.30/1.00/0.69/41.28/91.25	43.55/1.00/0.74/42.32/92.71	46.44/1.00/0.83/44.92/95.25
COCO	35.41/0.95/0.37/35.13/73.91	36.95/0.98/0.48/36.69/81.23	38.76/0.99/0.58/38.36/87.13	40.21/0.99/0.64/39.32/89.65	41.42/1.00/0.68/40.41/91.26	44.00/1.00/0.78/42.64/94.26
FFHQ	41.65/0.98/0.52/42.61/86.91	44.06/0.99/0.63/44.61/91.37	47.31/0.99/0.72/46.96/93.27	48.39/1.00/0.79/47.96/95.35	49.66/1.00/0.84/49.21/96.11	52.37/1.00/0.91/51.65/97.52
LSUN	37.39/0.96/0.39/36.95/74.96	39.25/0.98/0.49/38.76/81.61	42.26/0.99/0.60/41.32/87.69	43.79/0.99/0.65/42.51/89.92	45.43/1.00/0.69/43.82/91.55	48.92/1.00/0.79/47.39/94.39
RAISE	39.27/0.96/0.40/37.50/78.93	41.04/0.98/0.52/39.35/85.44	42.78/0.97/0.52/40.38/83.17	44.87/1.00/0.69/42.71/92.39	46.01/1.00/0.73/43.69/93.67	48.95/1.00/0.80/46.62/95.67
LAION	39.82/0.98/0.50/39.83/82.71	42.06/0.99/0.61/42.08/88.74	45.47/1.00/0.71/44.76/92.64	47.93/1.00/0.77/46.76/94.39	49.56/1.00/0.81/47.99/95.42	53.63/1.00/0.87/52.01/96.79
CelebA	38.64/0.98/0.58/39.76/85.49	41.63/0.99/0.72/42.45/91.35	46.28/1.00/0.81/45.62/94.37	48.52/1.00/0.86/47.75/95.86	50.56/1.00/0.90/49.81/96.67	54.28/1.00/0.95/53.33/97.86

Table 9. AUC, BA, FPR, and FNR for JPEG AI compression scenario for the [89]-A detector.

	Original format	BPP = 0.12	BPP = 0.25	BPP = 0.5	BPP = 0.75	BPP = 1.0	BPP = 2.0
	AUC / BA / FPR / FNR	AUC / BA / FPR / FNR	AUC / BA / FPR / FNR	AUC / BA / FPR / FNR	AUC / BA / FPR / FNR	AUC / BA / FPR / FNR	AUC / BA / FPR / FNR
Imagenet	0.88 / 0.70 / 0.07 / 0.53	0.58 / 0.55 / 0.59 / 0.32	0.66 / 0.61 / 0.46 / 0.33	0.73 / 0.66 / 0.24 / 0.45	0.78 / 0.68 / 0.17 / 0.48	0.81 / 0.68 / 0.11 / 0.54	0.86 / 0.64 / 0.04 / 0.68
COCO	0.92 / 0.79 / 0.07 / 0.35	0.78 / 0.67 / 0.52 / 0.15	0.83 / 0.73 / 0.41 / 0.14	0.89 / 0.81 / 0.17 / 0.20	0.92 / 0.84 / 0.10 / 0.23	0.92 / 0.82 / 0.10 / 0.26	0.93 / 0.75 / 0.04 / 0.46
CelebA	0.98 / 0.92 / 0.03 / 0.13	0.71 / 0.62 / 0.59 / 0.16	0.86 / 0.78 / 0.25 / 0.19	0.90 / 0.81 / 0.11 / 0.27	0.96 / 0.87 / 0.03 / 0.24	0.95 / 0.83 / 0.02 / 0.33	0.96 / 0.82 / 0.01 / 0.34
LSUN	0.99 / 0.89 / 0.00 / 0.22	0.72 / 0.63 / 0.55 / 0.19	0.83 / 0.75 / 0.27 / 0.23	0.88 / 0.78 / 0.10 / 0.34	0.93 / 0.81 / 0.05 / 0.33	0.95 / 0.82 / 0.02 / 0.34	0.98 / 0.80 / 0.00 / 0.40

can quickly inspect, regardless of the BPP value used in the second compression, the scores distribution of pristine samples will lie above the 0 threshold in the area corresponding to the scores distribution of single compressed 0.12 BPP images. On the contrary, Fig. 18c shows that if we first compress the samples with a high BPP value, the distribution of the scores will move accordingly to the BPP value of the second compression operation, i.e., a 0.12 BPP after a 2.0 BPP compression will shift the scores in the same area as a single 0.12 BPP compression. These results suggest that JPEG AI behaves similarly to standard compression formats in the sense that, if a strong compression has been applied to the input samples, the compressed images will likely still bear forensic artifacts relative to the first compression stage regardless of the BPP used in the second one.

Image splicing localization. In image splicing localization, the double compression usually does not interest the whole image. Indeed, it is rather common that only the spliced area indicated by the tampering mask $\mathbf{M}$ presents artifacts relative to a previous compression operation. This is because the source and target samples might have been saved with different formats or the same coding scheme but with one of the two images being processed with a more aggressive configuration.

We replicated this scenario by taking a spliced sample from an uncompressed dataset, i.e., DSO-1, and compressing this sample with all the BPP values considered in our experiments. After that, we created several spliced images where the spliced area was JPEG AI compressed at various BPP, and the surrounding content was uncompressed. We finally re-compressed all these images with BPP equal to 0.12 and 2.0. In this way, we are creating a mismatch in the spatial distribution of compression traces due to the spliced area bearing traces of the first JPEG AI compression, similar to the scenario analyzed in double JPEG compression.

Fig. 19 and Fig. 20 report the results of our double JPEG AI splicing operation together with the mask estimated by MMFusion. We also include the results of single-compressing the original format spliced image for reference. As we can quickly inspect, we can draw similar conclusions to the deepfake image detection experiments. In Fig. 20, the images were saved with BPP$= 2.0$, i.e., with very high quality. In this scenario, if the spliced area has been initially compressed with low BPP, MMFusion can detect this inconsistency and localize the spliced area with results much better than the reference single 2.0 BPP JPEG AI compression. On the other hand, in Fig. 19, the second compression stage at BPP$= 0.12$ likely erases all the traces relative to the first, hence making MMFusion deliver results very similar to a single JPEG AI compression. These results suggest that the inconsistency in the spatial distribution of JPEG AI artifacts might become a very powerful forensic instrument.

Table 10. AUC, BA, FPR, and FNR for JPEG AI compression scenario for the [89]-B detector.

	Original format	BPP = 0.12	BPP = 0.25	BPP = 0.5	BPP = 0.75	BPP = 1.0	BPP = 2.0
	AUC / BA / FPR / FNR	AUC / BA / FPR / FNR	AUC / BA / FPR / FNR	AUC / BA / FPR / FNR	AUC / BA / FPR / FNR	AUC / BA / FPR / FNR	AUC / BA / FPR / FNR
Imagenet	0.90 / 0.59 / 0.01 / 0.81	0.62 / 0.58 / 0.22 / 0.61	0.73 / 0.62 / 0.09 / 0.67	0.82 / 0.61 / 0.03 / 0.74	0.86 / 0.62 / 0.02 / 0.75	0.88 / 0.61 / 0.01 / 0.77	0.90 / 0.58 / 0.01 / 0.82
COCO	0.98 / 0.79 / 0.01 / 0.41	0.81 / 0.73 / 0.17 / 0.37	0.90 / 0.80 / 0.08 / 0.32	0.96 / 0.81 / 0.02 / 0.35	0.97 / 0.83 / 0.01 / 0.33	0.98 / 0.82 / 0.01 / 0.35	0.98 / 0.78 / 0.00 / 0.43
CelebA	0.95 / 0.81 / 0.01 / 0.37	0.71 / 0.60 / 0.06 / 0.74	0.83 / 0.62 / 0.02 / 0.74	0.90 / 0.71 / 0.01 / 0.56	0.93 / 0.74 / 0.01 / 0.50	0.93 / 0.76 / 0.01 / 0.48	0.94 / 0.76 / 0.00 / 0.48
LSUN	0.98 / 0.77 / 0.00 / 0.46	0.71 / 0.66 / 0.17 / 0.51	0.83 / 0.71 / 0.05 / 0.53	0.90 / 0.71 / 0.01 / 0.58	0.94 / 0.74 / 0.00 / 0.52	0.96 / 0.74 / 0.00 / 0.52	0.98 / 0.73 / 0.00 / 0.53

Table 11. AUC, BA, FPR, and FNR for JPEG AI compression scenario for the [43] detector.

	Original format	BPP = 0.12	BPP = 0.25	BPP = 0.5	BPP = 0.75	BPP = 1.0	BPP = 2.0
	AUC / BA / FPR / FNR	AUC / BA / FPR / FNR	AUC / BA / FPR / FNR	AUC / BA / FPR / FNR	AUC / BA / FPR / FNR	AUC / BA / FPR / FNR	AUC / BA / FPR / FNR
Imagenet	0.89 / 0.68 / 0.01 / 0.64	0.45 / 0.48 / 0.95 / 0.09	0.51 / 0.47 / 0.83 / 0.23	0.72 / 0.66 / 0.36 / 0.32	0.80 / 0.70 / 0.14 / 0.45	0.84 / 0.70 / 0.06 / 0.54	0.89 / 0.68 / 0.01 / 0.64
COCO	0.96 / 0.67 / 0.01 / 0.66	0.56 / 0.52 / 0.94 / 0.02	0.68 / 0.55 / 0.82 / 0.07	0.83 / 0.74 / 0.33 / 0.20	0.89 / 0.77 / 0.08 / 0.39	0.90 / 0.73 / 0.04 / 0.50	0.95 / 0.67 / 0.01 / 0.65
FFHQ	0.93 / 0.80 / 0.06 / 0.33	0.58 / 0.50 / 0.99 / 0.00	0.56 / 0.52 / 0.94 / 0.02	0.81 / 0.76 / 0.44 / 0.04	0.75 / 0.70 / 0.45 / 0.14	0.91 / 0.84 / 0.15 / 0.18	0.88 / 0.72 / 0.06 / 0.50

Table 12. AUC, BA, FPR, and FNR for JPEG AI compression scenario for the [33] detector.

	Original format	BPP = 0.12	BPP = 0.25	BPP = 0.5	BPP = 0.75	BPP = 1.0	BPP = 2.0
	AUC / BA / FPR / FNR	AUC / BA / FPR / FNR	AUC / BA / FPR / FNR	AUC / BA / FPR / FNR	AUC / BA / FPR / FNR	AUC / BA / FPR / FNR	AUC / BA / FPR / FNR
Imagenet	0.87 / 0.70 / 0.01 / 0.59	0.48 / 0.50 / 0.99 / 0.01	0.55 / 0.52 / 0.66 / 0.31	0.69 / 0.64 / 0.05 / 0.68	0.77 / 0.66 / 0.01 / 0.67	0.81 / 0.67 / 0.01 / 0.65	0.85 / 0.68 / 0.01 / 0.63
COCO	0.96 / 0.74 / 0.00 / 0.52	0.47 / 0.49 / 0.99 / 0.03	0.69 / 0.58 / 0.59 / 0.24	0.80 / 0.74 / 0.02 / 0.50	0.87 / 0.72 / 0.00 / 0.55	0.91 / 0.72 / 0.00 / 0.57	0.95 / 0.72 / 0.00 / 0.56
FFHQ	0.89 / 0.87 / 0.00 / 0.27	0.79 / 0.52 / 0.93 / 0.03	0.75 / 0.68 / 0.32 / 0.32	0.84 / 0.58 / 0.02 / 0.82	0.84 / 0.62 / 0.00 / 0.76	0.89 / 0.67 / 0.00 / 0.66	0.90 / 0.75 / 0.00 / 0.51

Table 13. AUC, BA, FPR, and FNR for JPEG AI compression scenario for the [71] detector.

	Original format	BPP = 0.12	BPP = 0.25	BPP = 0.5	BPP = 0.75	BPP = 1.0	BPP = 2.0
	AUC / BA / FPR / FNR	AUC / BA / FPR / FNR	AUC / BA / FPR / FNR	AUC / BA / FPR / FNR	AUC / BA / FPR / FNR	AUC / BA / FPR / FNR	AUC / BA / FPR / FNR
Imagenet	0.99 / 0.95 / 0.02 / 0.08	0.73 / 0.66 / 0.49 / 0.19	0.85 / 0.77 / 0.23 / 0.23	0.92 / 0.82 / 0.09 / 0.27	0.94 / 0.84 / 0.06 / 0.25	0.96 / 0.87 / 0.04 / 0.22	0.97 / 0.90 / 0.03 / 0.18
COCO	1.00 / 0.99 / 0.01 / 0.00	0.88 / 0.71 / 0.54 / 0.03	0.95 / 0.83 / 0.30 / 0.04	0.99 / 0.94 / 0.09 / 0.03	1.00 / 0.97 / 0.05 / 0.02	1.00 / 0.97 / 0.05 / 0.01	1.00 / 0.99 / 0.01 / 0.01
CelebA	0.99 / 0.96 / 0.07 / 0.02	0.91 / 0.82 / 0.30 / 0.07	0.96 / 0.89 / 0.12 / 0.09	0.97 / 0.91 / 0.11 / 0.06	0.98 / 0.93 / 0.09 / 0.04	0.98 / 0.93 / 0.10 / 0.04	0.98 / 0.93 / 0.08 / 0.05
LSUN	0.98 / 0.84 / 0.00 / 0.32	0.72 / 0.65 / 0.41 / 0.28	0.84 / 0.74 / 0.16 / 0.36	0.90 / 0.76 / 0.06 / 0.42	0.94 / 0.80 / 0.03 / 0.37	0.96 / 0.81 / 0.02 / 0.37	0.96 / 0.79 / 0.01 / 0.41
LAION	0.96 / 0.82 / 0.01 / 0.35	0.77 / 0.69 / 0.34 / 0.28	0.86 / 0.77 / 0.12 / 0.35	0.89 / 0.76 / 0.05 / 0.43	0.91 / 0.78 / 0.03 / 0.41	0.93 / 0.79 / 0.02 / 0.41	0.94 / 0.80 / 0.01 / 0.40

Table 14. AUC, BA, FPR, and FNR for JPEG AI compression scenario for the [35]-A detector.

	Original format	BPP = 0.12	BPP = 0.25	BPP = 0.5	BPP = 0.75	BPP = 1.0	BPP = 2.0
	AUC / BA / FPR / FNR	AUC / BA / FPR / FNR	AUC / BA / FPR / FNR	AUC / BA / FPR / FNR	AUC / BA / FPR / FNR	AUC / BA / FPR / FNR	AUC / BA / FPR / FNR
Imagenet	0.90 / 0.70 / 0.57 / 0.04	0.59 / 0.50 / 0.99 / 0.00	0.69 / 0.52 / 0.94 / 0.01	0.75 / 0.56 / 0.87 / 0.02	0.79 / 0.59 / 0.79 / 0.02	0.81 / 0.62 / 0.74 / 0.03	0.85 / 0.63 / 0.71 / 0.03
COCO	0.91 / 0.74 / 0.44 / 0.09	0.50 / 0.47 / 0.99 / 0.06	0.59 / 0.48 / 0.95 / 0.09	0.69 / 0.52 / 0.86 / 0.10	0.74 / 0.59 / 0.75 / 0.07	0.81 / 0.65 / 0.63 / 0.08	0.83 / 0.67 / 0.57 / 0.09
FFHQ	0.96 / 0.90 / 0.09 / 0.10	0.95 / 0.90 / 0.07 / 0.14	0.96 / 0.91 / 0.04 / 0.13	0.94 / 0.88 / 0.10 / 0.14	0.95 / 0.90 / 0.07 / 0.14	0.95 / 0.90 / 0.07 / 0.14	0.97 / 0.91 / 0.06 / 0.11
LSUN	0.95 / 0.87 / 0.18 / 0.09	0.50 / 0.51 / 0.99 / 0.00	0.52 / 0.52 / 0.94 / 0.02	0.59 / 0.52 / 0.87 / 0.09	0.65 / 0.55 / 0.81 / 0.10	0.64 / 0.54 / 0.81 / 0.12	0.81 / 0.64 / 0.68 / 0.04
LAION	0.96 / 0.80 / 0.37 / 0.03	0.52 / 0.50 / 0.99 / 0.01	0.64 / 0.51 / 0.97 / 0.01	0.73 / 0.54 / 0.91 / 0.01	0.75 / 0.56 / 0.87 / 0.02	0.75 / 0.55 / 0.89 / 0.02	0.80 / 0.57 / 0.83 / 0.02
RAISE	0.80 / 0.65 / 0.11 / 0.60	0.68 / 0.65 / 0.23 / 0.47	0.73 / 0.65 / 0.11 / 0.59	0.58 / 0.55 / 0.25 / 0.64	0.79 / 0.64 / 0.09 / 0.62	0.80 / 0.64 / 0.10 / 0.62	0.79 / 0.64 / 0.12 / 0.61

Table 15. AUC, BA, FPR, and FNR for JPEG AI compression scenario for the [35]-B detector.

	Original format	BPP = 0.12	BPP = 0.25	BPP = 0.5	BPP = 0.75	BPP = 1.0	BPP = 2.0
	AUC / BA / FPR / FNR	AUC / BA / FPR / FNR	AUC / BA / FPR / FNR	AUC / BA / FPR / FNR	AUC / BA / FPR / FNR	AUC / BA / FPR / FNR	AUC / BA / FPR / FNR
Imagenet	0.76 / 0.68 / 0.42 / 0.21	0.61 / 0.51 / 0.98 / 0.00	0.68 / 0.53 / 0.94 / 0.01	0.71 / 0.55 / 0.87 / 0.03	0.72 / 0.57 / 0.82 / 0.03	0.74 / 0.59 / 0.78 / 0.04	0.75 / 0.60 / 0.74 / 0.06
COCO	0.86 / 0.77 / 0.32 / 0.14	0.53 / 0.49 / 0.98 / 0.04	0.65 / 0.51 / 0.92 / 0.06	0.73 / 0.55 / 0.83 / 0.08	0.77 / 0.58 / 0.76 / 0.07	0.80 / 0.62 / 0.67 / 0.08	0.83 / 0.68 / 0.55 / 0.10
FFHQ	0.88 / 0.77 / 0.10 / 0.36	0.96 / 0.86 / 0.21 / 0.08	0.96 / 0.88 / 0.15 / 0.09	0.95 / 0.88 / 0.14 / 0.11	0.94 / 0.87 / 0.11 / 0.15	0.94 / 0.87 / 0.10 / 0.17	0.95 / 0.89 / 0.09 / 0.14
LSUN	0.79 / 0.68 / 0.49 / 0.14	0.52 / 0.51 / 0.98 / 0.01	0.56 / 0.52 / 0.93 / 0.03	0.62 / 0.53 / 0.85 / 0.08	0.67 / 0.55 / 0.80 / 0.09	0.66 / 0.55 / 0.79 / 0.11	0.72 / 0.59 / 0.73 / 0.08
RAISE	0.86 / 0.77 / 0.15 / 0.31	0.76 / 0.67 / 0.47 / 0.20	0.79 / 0.72 / 0.29 / 0.27	0.74 / 0.68 / 0.35 / 0.29	0.84 / 0.75 / 0.20 / 0.29	0.84 / 0.76 / 0.19 / 0.29	0.85 / 0.76 / 0.17 / 0.32

Table 16. AUC, BA, FPR, and FNR for JPEG AI compression scenario for the [64] detector.

	Original format	BPP = 0.12	BPP = 0.25	BPP = 0.5	BPP = 0.75	BPP = 1.0	BPP = 2.0
	AUC / BA / FPR / FNR	AUC / BA / FPR / FNR	AUC / BA / FPR / FNR	AUC / BA / FPR / FNR	AUC / BA / FPR / FNR	AUC / BA / FPR / FNR	AUC / BA / FPR / FNR
CelebA	1.00 / 1.00 / 0.00 / 0.00	0.81 / 0.50 / 1.00 / 0.00	0.92 / 0.54 / 0.93 / 0.00	0.98 / 0.91 / 0.18 / 0.00	1.00 / 0.99 / 0.02 / 0.00	1.00 / 0.99 / 0.01 / 0.00	1.00 / 1.00 / 0.00 / 0.00
FFHQ	1.00 / 1.00 / 0.00 / 0.00	0.97 / 0.79 / 0.39 / 0.03	0.99 / 0.94 / 0.07 / 0.05	1.00 / 0.99 / 0.00 / 0.01	1.00 / 1.00 / 0.00 / 0.00	1.00 / 1.00 / 0.00 / 0.00	1.00 / 1.00 / 0.00 / 0.00
Imagenet	0.71 / 0.62 / 0.13 / 0.64	0.51 / 0.50 / 0.72 / 0.28	0.53 / 0.52 / 0.50 / 0.47	0.55 / 0.54 / 0.39 / 0.54	0.57 / 0.56 / 0.33 / 0.56	0.59 / 0.56 / 0.28 / 0.60	0.64 / 0.59 / 0.23 / 0.59
LAION	0.72 / 0.68 / 0.18 / 0.46	0.61 / 0.59 / 0.51 / 0.32	0.63 / 0.60 / 0.39 / 0.41	0.69 / 0.63 / 0.32 / 0.42	0.72 / 0.66 / 0.25 / 0.44	0.73 / 0.67 / 0.23 / 0.43	0.73 / 0.66 / 0.22 / 0.46
LSUN	0.83 / 0.76 / 0.12 / 0.37	0.50 / 0.51 / 0.82 / 0.16	0.61 / 0.59 / 0.55 / 0.27	0.58 / 0.55 / 0.50 / 0.40	0.63 / 0.59 / 0.38 / 0.44	0.63 / 0.60 / 0.32 / 0.49	0.73 / 0.68 / 0.20 / 0.44
RAISE	0.86 / 0.80 / 0.02 / 0.38	0.63 / 0.59 / 0.34 / 0.48	0.75 / 0.68 / 0.14 / 0.51	0.83 / 0.75 / 0.03 / 0.48	0.81 / 0.75 / 0.04 / 0.46	0.82 / 0.76 / 0.02 / 0.46	0.81 / 0.78 / 0.03 / 0.42

Table 17. AUC, BA, FPR, and FNR for JPEG AI compression scenario for the [82] detector.

	Original format	BPP = 0.12	BPP = 0.25	BPP = 0.5	BPP = 0.75	BPP = 1.0	BPP = 2.0
	AUC / BA / FPR / FNR	AUC / BA / FPR / FNR	AUC / BA / FPR / FNR	AUC / BA / FPR / FNR	AUC / BA / FPR / FNR	AUC / BA / FPR / FNR	AUC / BA / FPR / FNR
Imagenet	0.94 / 0.84 / 0.30 / 0.01	0.50 / 0.51 / 0.99 / 0.00	0.46 / 0.51 / 0.98 / 0.00	0.44 / 0.51 / 0.98 / 0.00	0.46 / 0.51 / 0.98 / 0.01	0.47 / 0.51 / 0.97 / 0.01	0.52 / 0.51 / 0.97 / 0.01
COCO	0.91 / 0.82 / 0.34 / 0.01	0.67 / 0.50 / 1.00 / 0.00	0.62 / 0.50 / 0.99 / 0.00	0.60 / 0.51 / 0.99 / 0.00	0.63 / 0.51 / 0.98 / 0.00	0.58 / 0.51 / 0.97 / 0.00	0.57 / 0.51 / 0.97 / 0.00
CelebA	1.00 / 0.99 / 0.01 / 0.00	0.67 / 0.50 / 1.00 / 0.00	0.74 / 0.50 / 1.00 / 0.00	0.60 / 0.50 / 1.00 / 0.00	0.81 / 0.50 / 1.00 / 0.00	0.77 / 0.50 / 1.00 / 0.00	0.92 / 0.50 / 1.00 / 0.00
LSUN	1.00 / 0.99 / 0.00 / 0.03	0.64 / 0.50 / 1.00 / 0.00	0.61 / 0.50 / 1.00 / 0.00	0.53 / 0.50 / 0.99 / 0.00	0.55 / 0.50 / 0.99 / 0.00	0.54 / 0.50 / 0.99 / 0.01	0.61 / 0.51 / 0.97 / 0.02
LAION	0.99 / 0.97 / 0.02 / 0.05	0.80 / 0.51 / 0.97 / 0.00	0.75 / 0.51 / 0.97 / 0.00	0.75 / 0.52 / 0.96 / 0.00	0.74 / 0.52 / 0.95 / 0.01	0.79 / 0.53 / 0.92 / 0.01	0.82 / 0.55 / 0.89 / 0.01

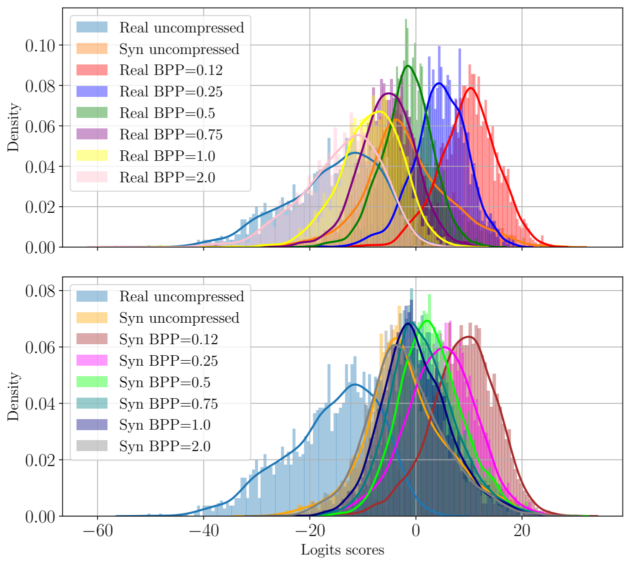

(a) JPEG AI scores distribution over the Imagenet dataset.

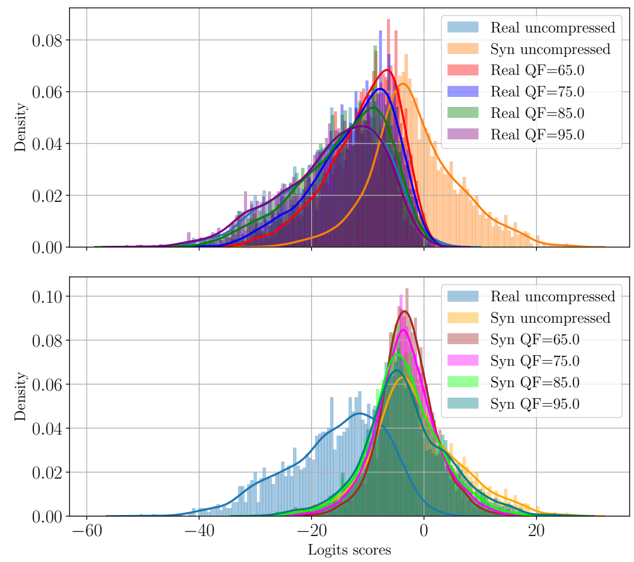

(b) JPEG scores distribution over the Imagenet dataset.

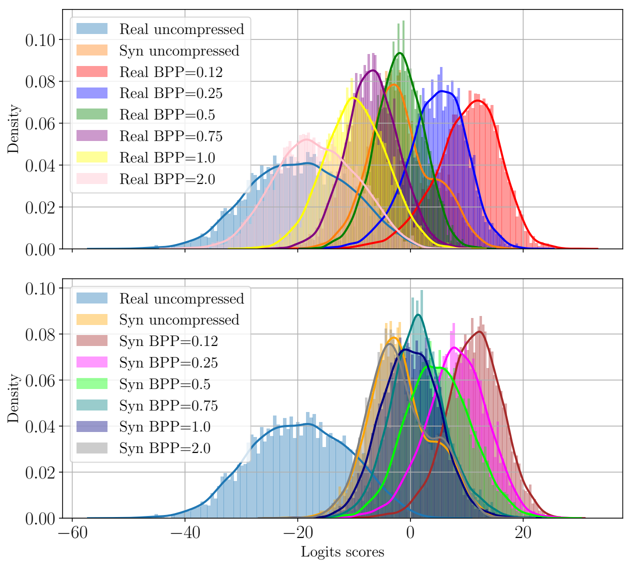

(c) JPEG AI scores distribution over the COCO dataset.

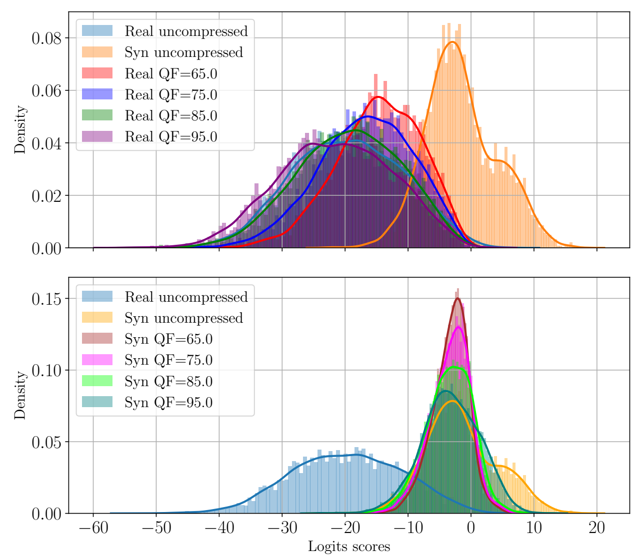

(d) JPEG scores distribution over the COCO dataset.

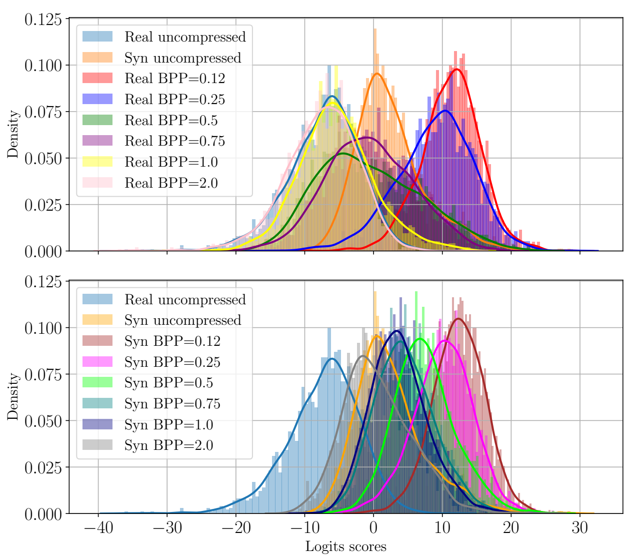

(e) JPEG AI scores distribution over the FFHQ dataset.

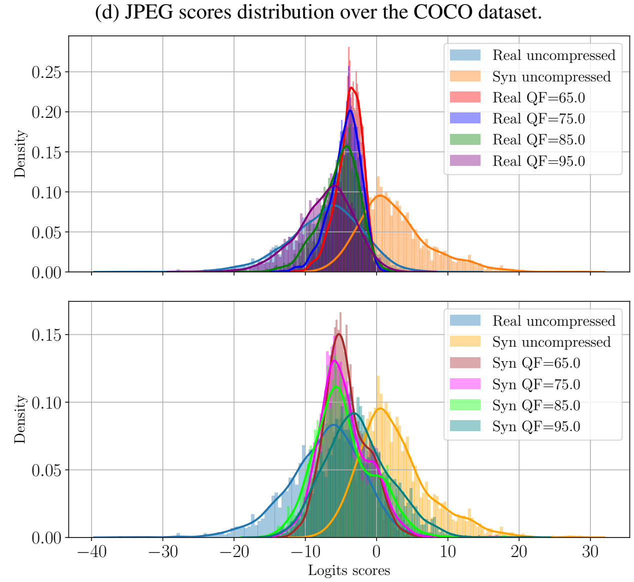

(f) JPEG scores distribution over the FFHQ dataset.

Figure 7. Scores distribution over the different datasets of the [43] detector.

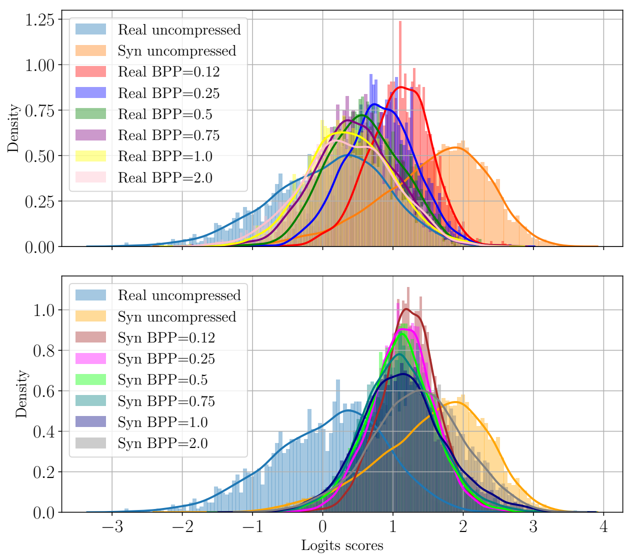

(a) JPEG AI scores distribution over the Imagenet dataset.

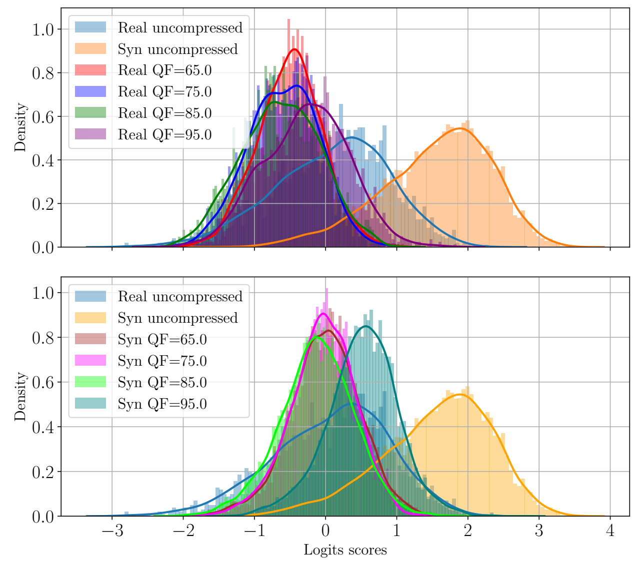

(b) JPEG scores distribution over the Imagenet dataset.

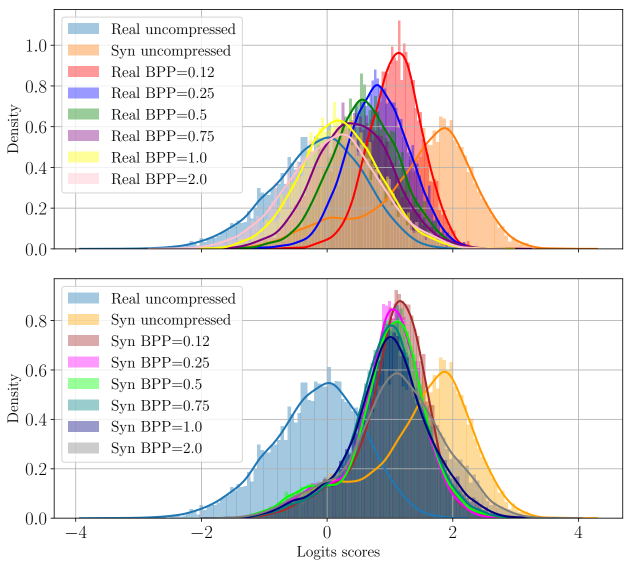

(c) JPEG AI scores distribution over the COCO dataset.

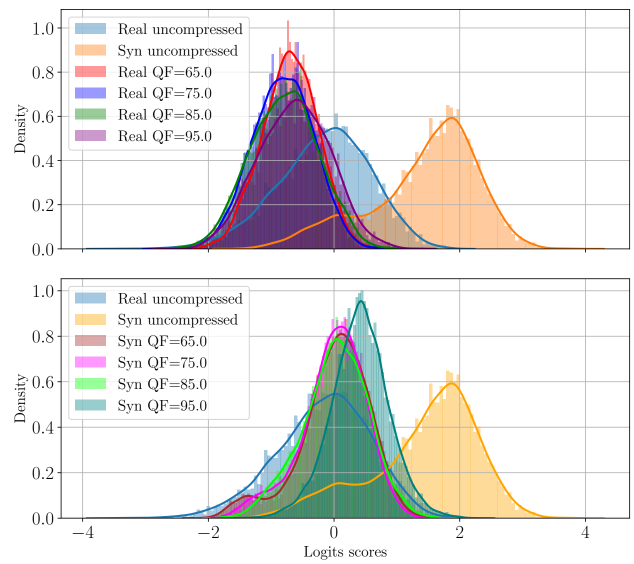

(d) JPEG scores distribution over the COCO dataset.

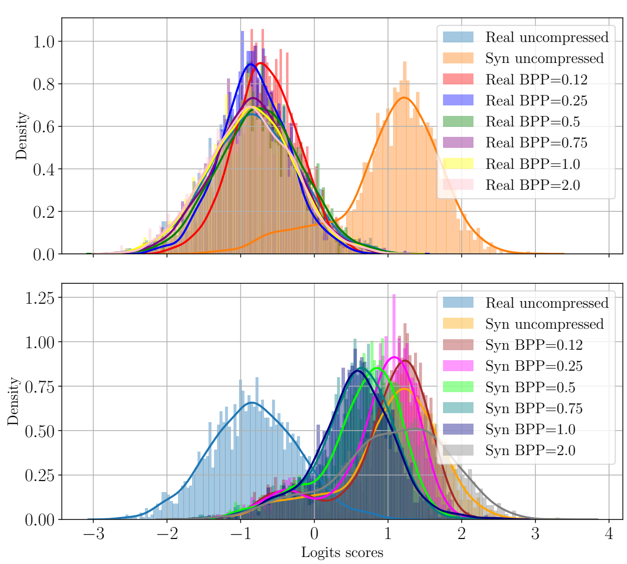

(e) JPEG AI scores distribution over the FFHQ dataset.

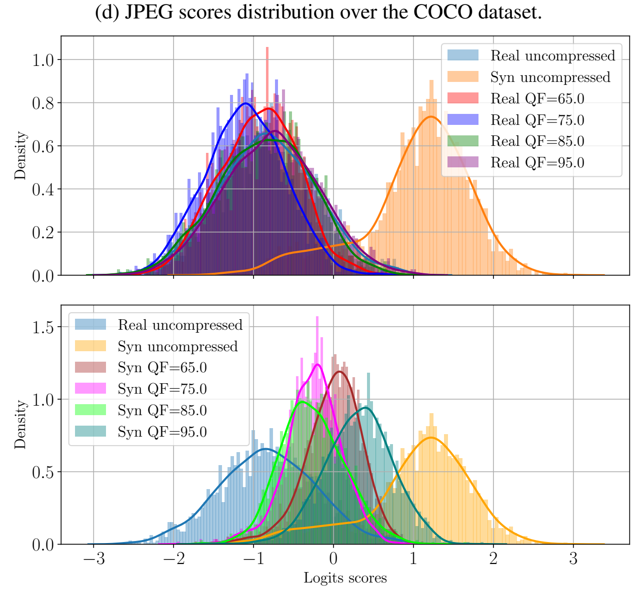

(f) JPEG scores distribution over the FFHQ dataset.

Figure 8. Scores distribution over the ImageNet, COCO, and FFHQ datasets of the [35]-A detector.

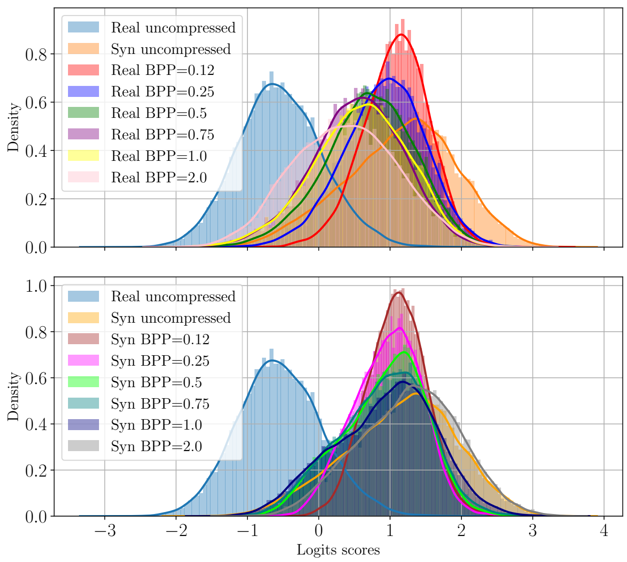

(a) JPEG AI scores distribution over the LSUN dataset.

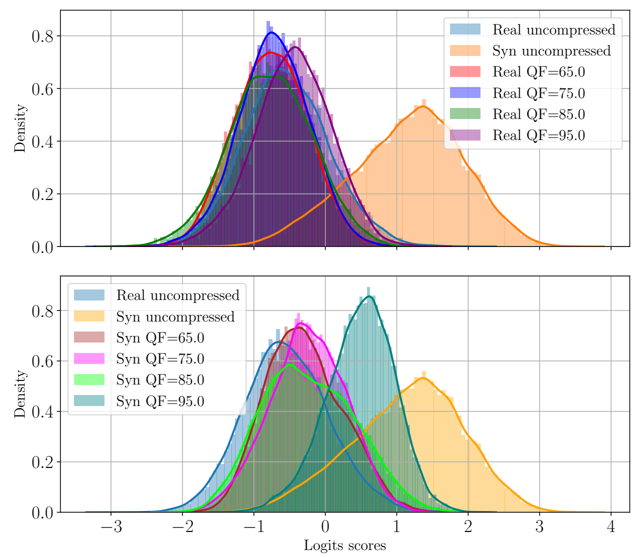

(b) JPEG scores distribution over the LSUN dataset.

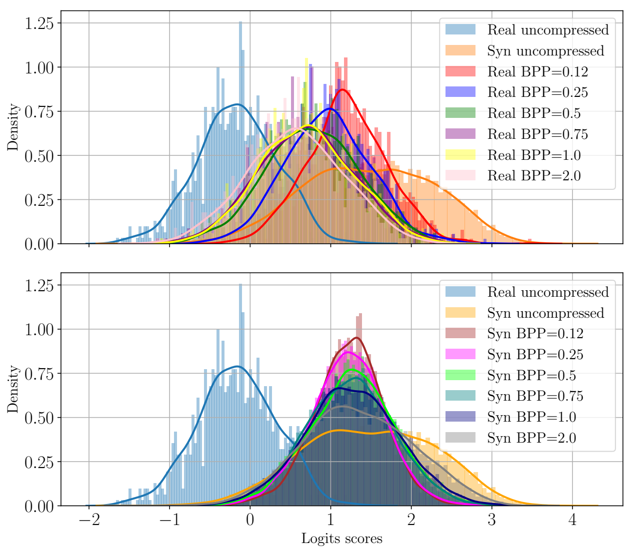

(c) JPEG AI scores distribution over the LAION dataset.

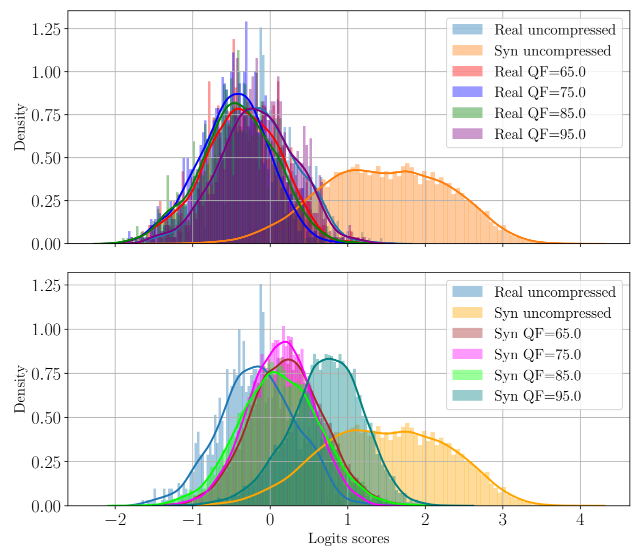

(d) JPEG scores distribution over the LAION dataset.

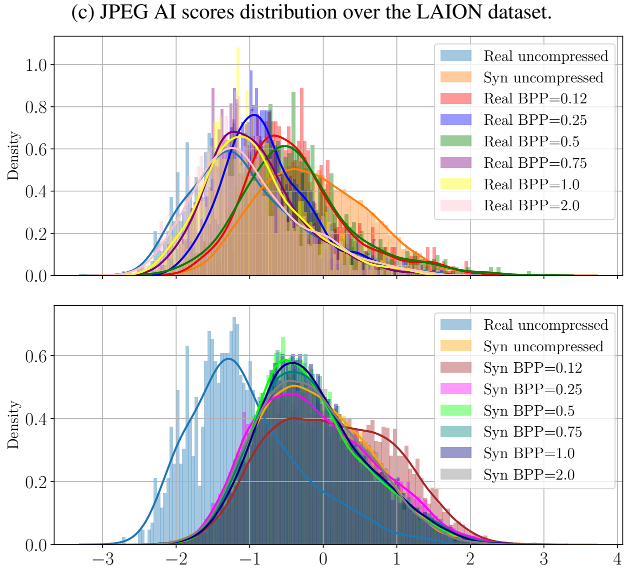

(e) JPEG AI scores distribution over the RAISE dataset.

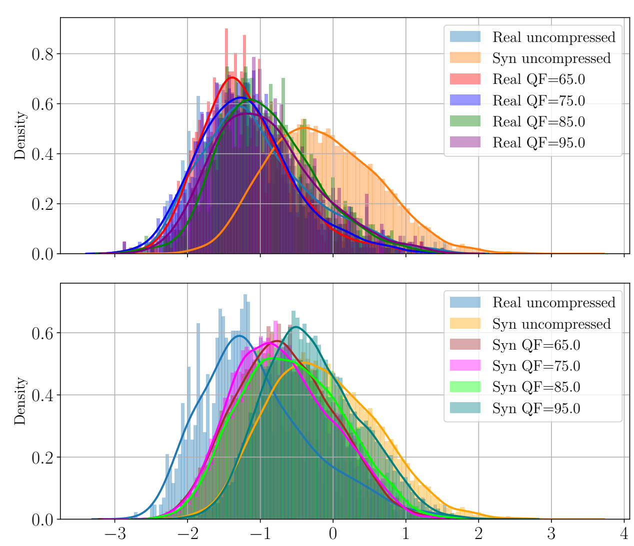

(f) JPEG scores distribution over the RAISE dataset.

Figure 9. Scores distribution over the LSUN, LAION, and RAISE datasets of the [35]-A detector.

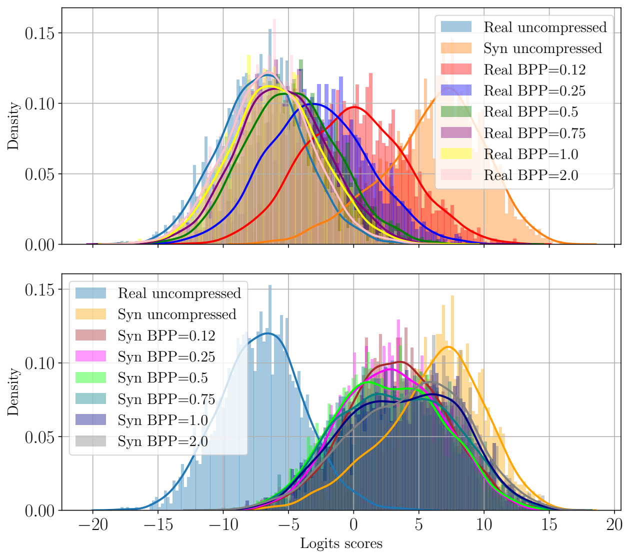

(a) JPEG AI scores distribution over the Imagenet dataset.

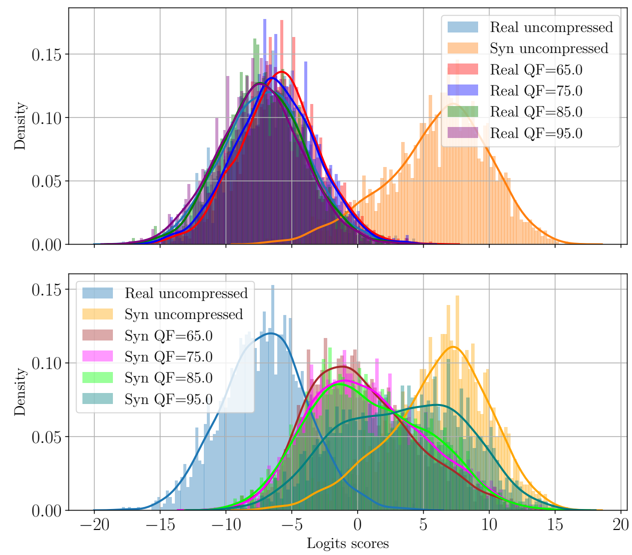

(b) JPEG scores distribution over the Imagenet dataset.

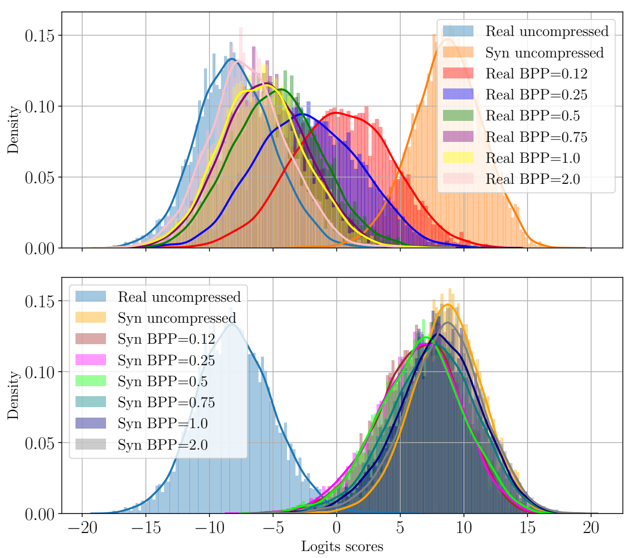

(c) JPEG AI scores distribution over the COCO dataset.

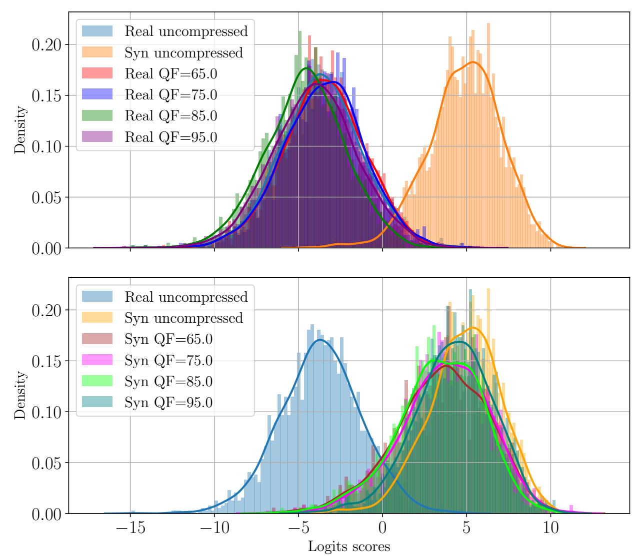

(d) JPEG scores distribution over the COCO dataset.

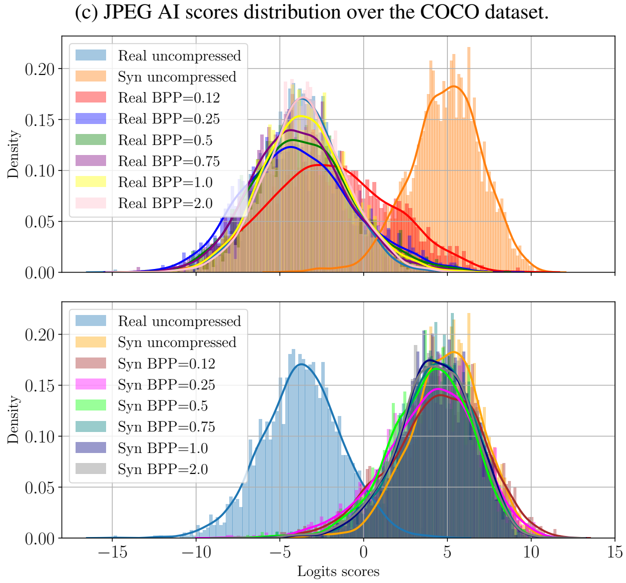

(e) JPEG AI scores distribution over the CelebA dataset.

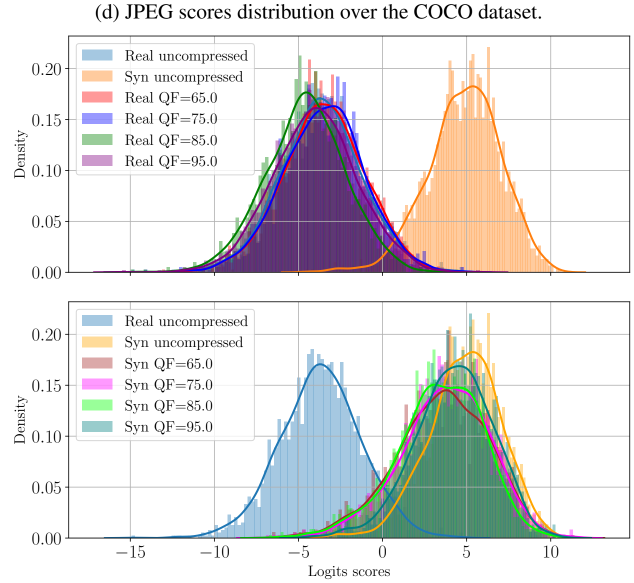

(f) JPEG scores distribution over the CelebA dataset.

Figure 10. Scores distribution over the Imagenet, COCO, and CelebA datasets of the [71] detector.

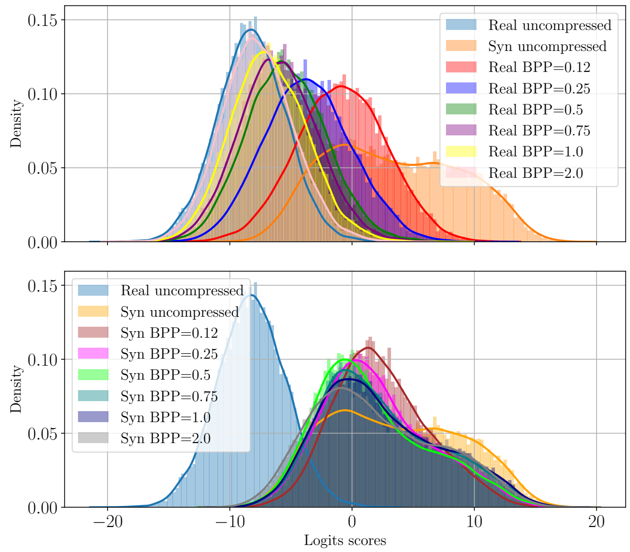

(a) JPEG AI scores distribution over the LSUN dataset.

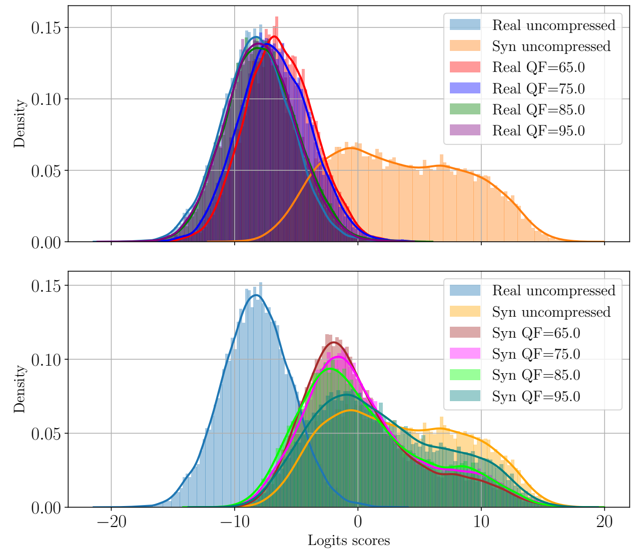

(b) JPEG scores distribution over the LSUN dataset.

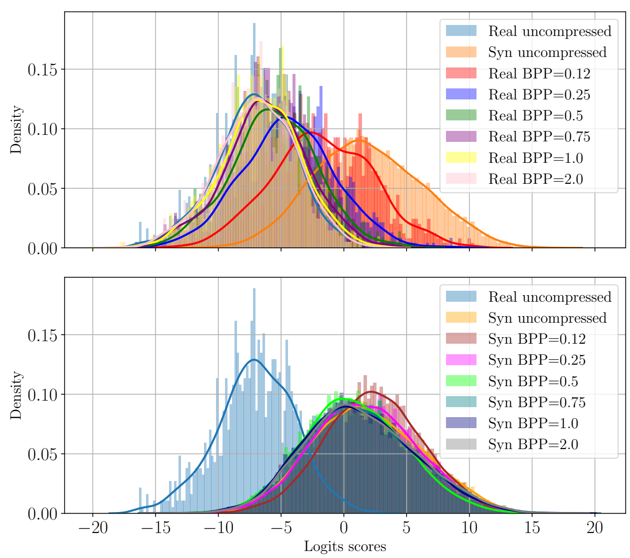

(c) JPEG AI scores distribution over the LAION dataset.

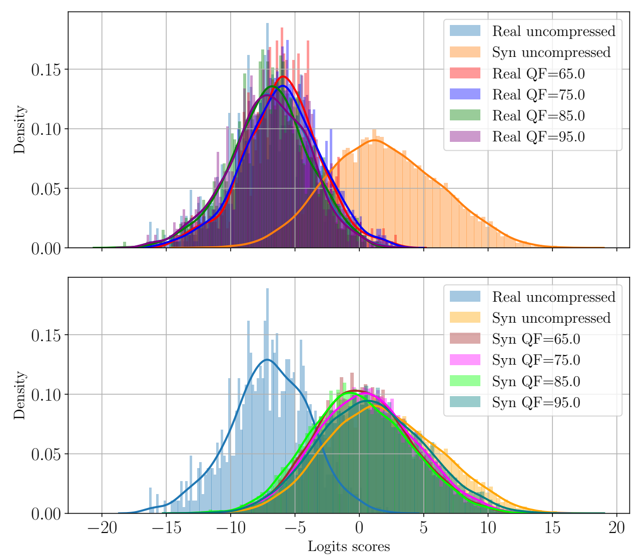

(d) JPEG scores distribution over the LAION dataset.

Figure 11. Scores distribution over the LSUN and LAION datasets of the [71] detector.

Table 18. AUC, BA, FPR, and FNR for the JPEG compression scenario for the [89]-A detector.

	Original format	QF = 65	QF = 75	QF = 85	QF = 95
	AUC / BA / FPR / FNR	AUC / BA / FPR / FNR	AUC / BA / FPR / FNR	AUC / BA / FPR / FNR	AUC / BA / FPR / FNR
Imagenet	0.88 / 0.70 / 0.07 / 0.53	0.88 / 0.60 / 0.01 / 0.79	0.88 / 0.60 / 0.01 / 0.79	0.89 / 0.60 / 0.01 / 0.80	0.89 / 0.62 / 0.01 / 0.74
COCO	0.92 / 0.79 / 0.07 / 0.35	0.96 / 0.70 / 0.00 / 0.59	0.96 / 0.69 / 0.00 / 0.61	0.96 / 0.68 / 0.00 / 0.64	0.96 / 0.70 / 0.01 / 0.60
CelebA	0.98 / 0.92 / 0.03 / 0.13	0.89 / 0.76 / 0.04 / 0.44	0.89 / 0.75 / 0.04 / 0.47	0.91 / 0.75 / 0.02 / 0.47	0.93 / 0.79 / 0.02 / 0.40
LSUN	0.99 / 0.89 / 0.00 / 0.22	0.95 / 0.72 / 0.00 / 0.56	0.96 / 0.74 / 0.00 / 0.53	0.97 / 0.75 / 0.00 / 0.50	0.99 / 0.79 / 0.00 / 0.42

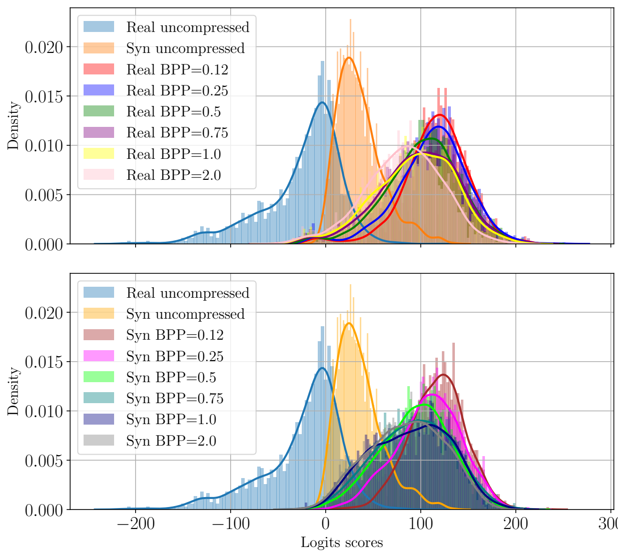

(a) JPEG AI scores distribution over the Imagenet dataset.

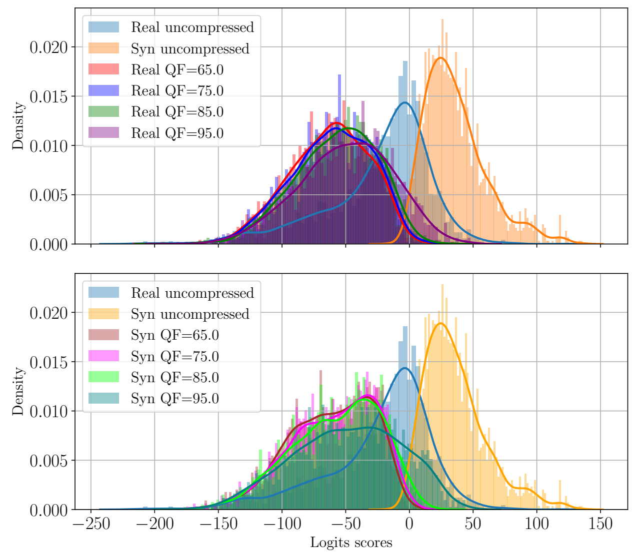

(b) JPEG scores distribution over the Imagenet dataset.

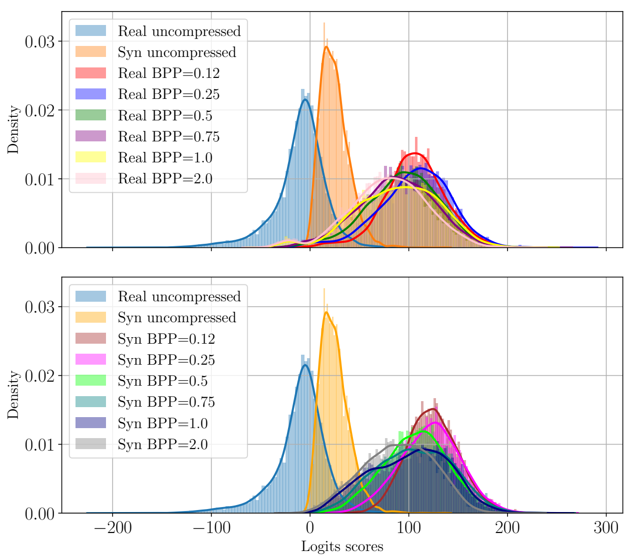

(c) JPEG AI scores distribution over the COCO dataset.

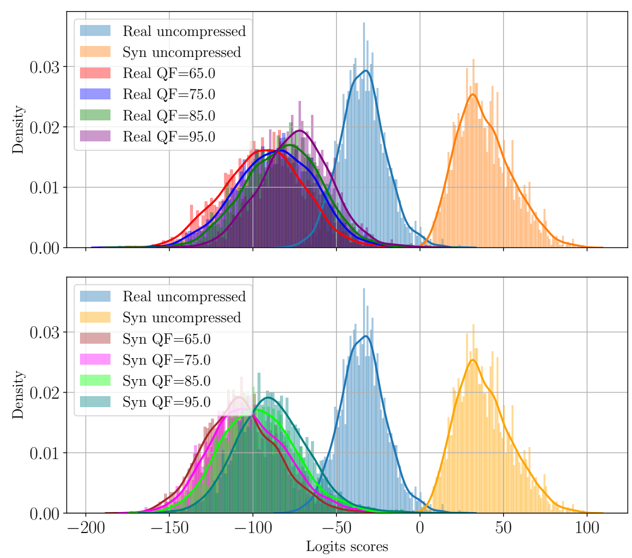

(d) JPEG scores distribution over the COCO dataset.

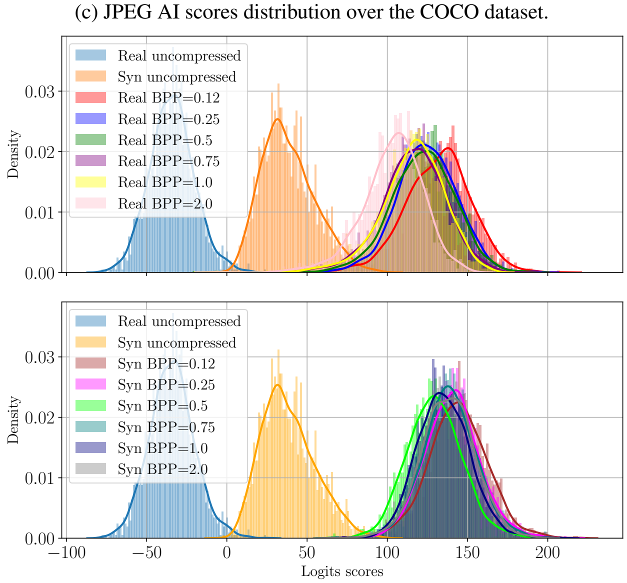

(e) JPEG AI scores distribution over the CelebA dataset.

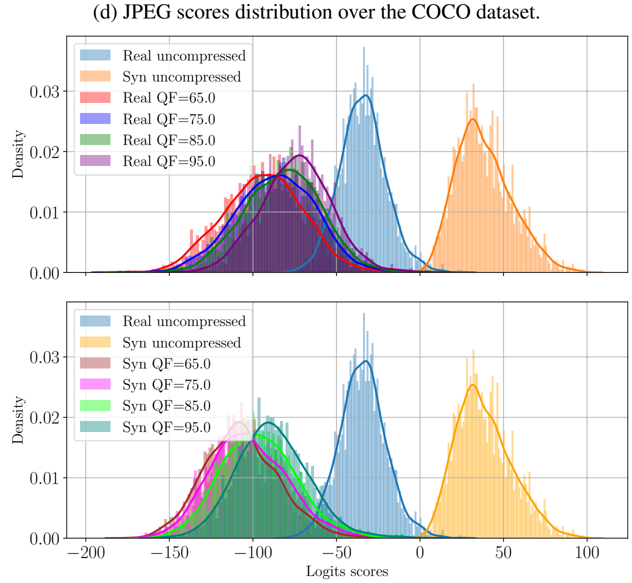

(f) JPEG scores distribution over the CelebA dataset.

Figure 12. Scores distribution over the Imagenet, COCO, and CelebA datasets of the [82] detector.

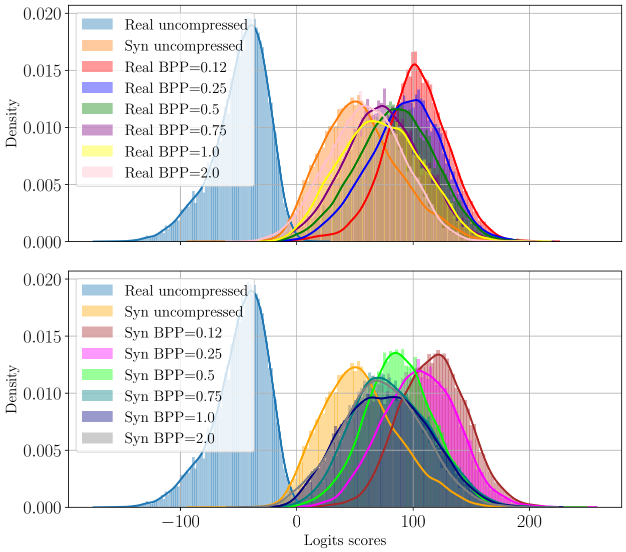

(a) JPEG AI scores distribution over the LSUN dataset.

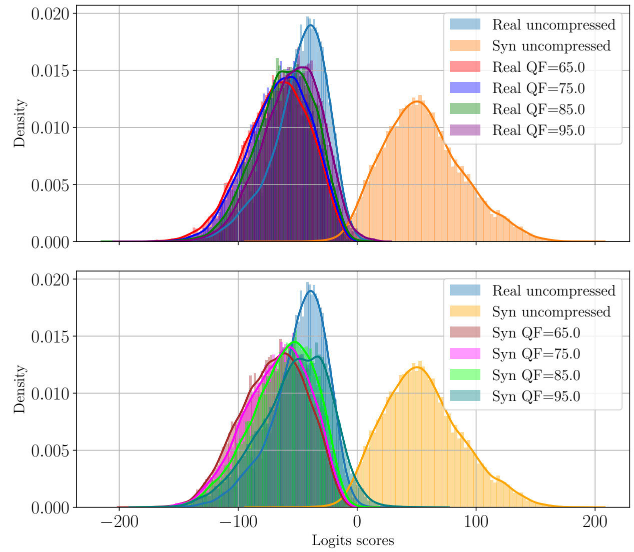

(b) JPEG scores distribution over the LSUN dataset.

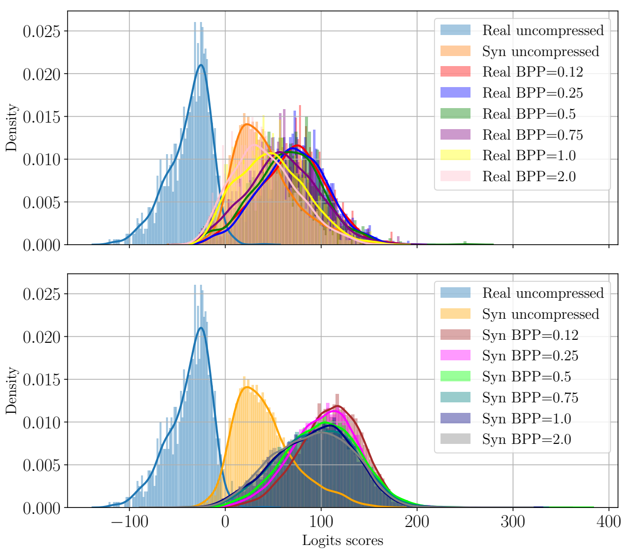

(c) JPEG AI scores distribution over the LAION dataset.

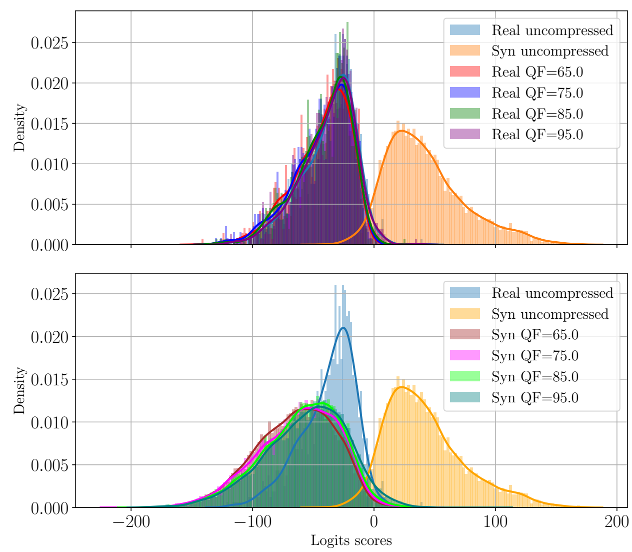

(d) JPEG scores distribution over the LAION dataset.

Figure 13. Scores distribution over the LSUN and LAION datasets of the [82] detector.

Table 19. AUC, BA, FPR, and FNR for the JPEG compression scenario for the [89]-B detector.

	Original format	QF = 65	QF = 75	QF = 85	QF = 95
	AUC / BA / FPR / FNR	AUC / BA / FPR / FNR	AUC / BA / FPR / FNR	AUC / BA / FPR / FNR	AUC / BA / FPR / FNR
Imagenet	0.90 / 0.59 / 0.01 / 0.81	0.89 / 0.57 / 0.01 / 0.86	0.89 / 0.57 / 0.00 / 0.86	0.90 / 0.57 / 0.01 / 0.86	0.90 / 0.57 / 0.01 / 0.85
COCO	0.98 / 0.79 / 0.01 / 0.41	0.99 / 0.75 / 0.00 / 0.49	0.99 / 0.75 / 0.00 / 0.50	0.99 / 0.75 / 0.00 / 0.51	0.99 / 0.76 / 0.00 / 0.48
CelebA	0.95 / 0.81 / 0.01 / 0.37	0.91 / 0.73 / 0.01 / 0.52	0.92 / 0.74 / 0.01 / 0.50	0.92 / 0.75 / 0.01 / 0.50	0.93 / 0.76 / 0.01 / 0.47
LSUN	0.98 / 0.77 / 0.00 / 0.46	0.96 / 0.69 / 0.00 / 0.61	0.96 / 0.70 / 0.00 / 0.59	0.97 / 0.71 / 0.00 / 0.58	0.98 / 0.73 / 0.00 / 0.54

Table 20. AUC, BA, FPR, and FNR for the JPEG compression scenario for the [43] detector.

	Original format	QF = 65	QF = 75	QF = 85	QF = 95
	AUC / BA / FPR / FNR	AUC / BA / FPR / FNR	AUC / BA / FPR / FNR	AUC / BA / FPR / FNR	AUC / BA / FPR / FNR
Imagenet	0.89 / 0.68 / 0.01 / 0.64	0.84 / 0.62 / 0.01 / 0.76	0.85 / 0.62 / 0.01 / 0.75	0.86 / 0.63 / 0.00 / 0.74	0.88 / 0.64 / 0.00 / 0.71
COCO	0.96 / 0.67 / 0.01 / 0.66	0.95 / 0.55 / 0.00 / 0.89	0.96 / 0.56 / 0.00 / 0.87	0.97 / 0.59 / 0.00 / 0.82	0.97 / 0.63 / 0.00 / 0.75
FFHQ	0.93 / 0.80 / 0.06 / 0.33	0.42 / 0.55 / 0.00 / 0.91	0.45 / 0.56 / 0.00 / 0.88	0.52 / 0.58 / 0.01 / 0.84	0.77 / 0.62 / 0.02 / 0.74

Table 21. AUC, BA, FPR, and FNR for the JPEG compression scenario for the [33] detector.

	Original format	QF = 65	QF = 75	QF = 85	QF = 95
	AUC / BA / FPR / FNR	AUC / BA / FPR / FNR	AUC / BA / FPR / FNR	AUC / BA / FPR / FNR	AUC / BA / FPR / FNR
Imagenet	0.87 / 0.70 / 0.01 / 0.59	0.83 / 0.72 / 0.04 / 0.53	0.83 / 0.71 / 0.03 / 0.56	0.84 / 0.70 / 0.01 / 0.59	0.87 / 0.69 / 0.01 / 0.61
COCO	0.96 / 0.74 / 0.00 / 0.52	0.98 / 0.81 / 0.00 / 0.37	0.98 / 0.79 / 0.00 / 0.42	0.98 / 0.75 / 0.00 / 0.50	0.97 / 0.73 / 0.00 / 0.54
FFHQ	0.89 / 0.87 / 0.00 / 0.27	0.93 / 0.81 / 0.28 / 0.10	0.93 / 0.84 / 0.19 / 0.13	0.92 / 0.87 / 0.06 / 0.20	0.91 / 0.86 / 0.00 / 0.28

Table 22. AUC, BA, FPR, and FNR for the JPEG compression scenario for the [71] detector.

	Original format	QF = 65	QF = 75	QF = 85	QF = 95
	AUC / BA / FPR / FNR	AUC / BA / FPR / FNR	AUC / BA / FPR / FNR	AUC / BA / FPR / FNR	AUC / BA / FPR / FNR
Imagenet	0.99 / 0.95 / 0.02 / 0.08	0.90 / 0.72 / 0.03 / 0.53	0.91 / 0.75 / 0.02 / 0.47	0.94 / 0.76 / 0.01 / 0.46	0.97 / 0.86 / 0.01 / 0.28
COCO	1.00 / 0.99 / 0.01 / 0.00	0.99 / 0.93 / 0.01 / 0.13	0.99 / 0.95 / 0.01 / 0.10	1.00 / 0.96 / 0.01 / 0.07	1.00 / 0.98 / 0.01 / 0.03
CelebA	0.99 / 0.96 / 0.07 / 0.02	0.97 / 0.91 / 0.07 / 0.10	0.97 / 0.92 / 0.07 / 0.09	0.99 / 0.94 / 0.03 / 0.10	0.99 / 0.95 / 0.06 / 0.04
LSUN	0.98 / 0.84 / 0.00 / 0.32	0.91 / 0.71 / 0.01 / 0.58	0.92 / 0.72 / 0.01 / 0.54	0.94 / 0.72 / 0.01 / 0.55	0.96 / 0.79 / 0.00 / 0.42
LAION	0.96 / 0.82 / 0.01 / 0.35	0.91 / 0.75 / 0.03 / 0.48	0.91 / 0.76 / 0.02 / 0.45	0.92 / 0.74 / 0.01 / 0.52	0.94 / 0.78 / 0.01 / 0.42

Table 23. AUC, BA, FPR, and FNR for the JPEG compression scenario for the [35]-A detector.

	Original format	QF = 65	QF = 75	QF = 85	QF = 95
	AUC / BA / FPR / FNR	AUC / BA / FPR / FNR	AUC / BA / FPR / FNR	AUC / BA / FPR / FNR	AUC / BA / FPR / FNR
Imagenet	0.90 / 0.70 / 0.57 / 0.04	0.77 / 0.69 / 0.12 / 0.50	0.79 / 0.68 / 0.11 / 0.52	0.75 / 0.64 / 0.13 / 0.59	0.85 / 0.76 / 0.34 / 0.14
COCO	0.91 / 0.74 / 0.44 / 0.09	0.85 / 0.75 / 0.05 / 0.44	0.87 / 0.74 / 0.04 / 0.47	0.85 / 0.73 / 0.08 / 0.46	0.92 / 0.85 / 0.13 / 0.17
FFHQ	0.96 / 0.90 / 0.09 / 0.10	0.94 / 0.75 / 0.03 / 0.46	0.92 / 0.61 / 0.01 / 0.77	0.80 / 0.60 / 0.06 / 0.75	0.93 / 0.84 / 0.10 / 0.23
LSUN	0.95 / 0.87 / 0.18 / 0.09	0.73 / 0.61 / 0.07 / 0.72	0.74 / 0.63 / 0.07 / 0.67	0.72 / 0.63 / 0.10 / 0.64	0.90 / 0.82 / 0.20 / 0.16
LAION	0.96 / 0.80 / 0.37 / 0.03	0.80 / 0.71 / 0.24 / 0.33	0.84 / 0.74 / 0.14 / 0.37	0.77 / 0.69 / 0.21 / 0.41	0.90 / 0.78 / 0.37 / 0.08
RAISE	0.80 / 0.65 / 0.11 / 0.60	0.72 / 0.56 / 0.05 / 0.82	0.71 / 0.56 / 0.06 / 0.82	0.64 / 0.56 / 0.10 / 0.78	0.75 / 0.60 / 0.11 / 0.68

Table 24. AUC, BA, FPR, and FNR for the JPEG compression scenario for the [35]-B detector.

	Original format	QF = 65	QF = 75	QF = 85	QF = 95
	AUC / BA / FPR / FNR	AUC / BA / FPR / FNR	AUC / BA / FPR / FNR	AUC / BA / FPR / FNR	AUC / BA / FPR / FNR
Imagenet	0.76 / 0.68 / 0.42 / 0.21	0.66 / 0.62 / 0.40 / 0.36	0.71 / 0.66 / 0.36 / 0.33	0.64 / 0.60 / 0.32 / 0.48	0.69 / 0.64 / 0.52 / 0.20
COCO	0.86 / 0.77 / 0.32 / 0.14	0.81 / 0.73 / 0.33 / 0.22	0.86 / 0.77 / 0.19 / 0.26	0.82 / 0.73 / 0.17 / 0.37	0.83 / 0.75 / 0.30 / 0.20
FFHQ	0.88 / 0.77 / 0.10 / 0.36	0.87 / 0.72 / 0.08 / 0.47	0.77 / 0.65 / 0.18 / 0.52	0.63 / 0.54 / 0.14 / 0.77	0.83 / 0.67 / 0.11 / 0.54
LSUN	0.79 / 0.68 / 0.49 / 0.14	0.70 / 0.64 / 0.36 / 0.35	0.70 / 0.65 / 0.39 / 0.30	0.67 / 0.62 / 0.38 / 0.37	0.80 / 0.70 / 0.48 / 0.12
RAISE	0.86 / 0.77 / 0.15 / 0.31	0.78 / 0.70 / 0.22 / 0.37	0.76 / 0.69 / 0.21 / 0.40	0.74 / 0.68 / 0.22 / 0.41	0.84 / 0.75 / 0.20 / 0.31

Table 25. AUC, BA, FPR, and FNR for the JPEG compression scenario for the [64] detector.

	Original format	QF = 65	QF = 75	QF = 85	QF = 95
	AUC / BA / FPR / FNR	AUC / BA / FPR / FNR	AUC / BA / FPR / FNR	AUC / BA / FPR / FNR	AUC / BA / FPR / FNR
CelebA	1.00 / 1.00 / 0.00 / 0.00	1.00 / 1.00 / 0.01 / 0.00	1.00 / 1.00 / 0.00 / 0.00	1.00 / 1.00 / 0.00 / 0.00	1.00 / 1.00 / 0.00 / 0.00
FFHQ	1.00 / 1.00 / 0.00 / 0.00	1.00 / 1.00 / 0.00 / 0.01	1.00 / 1.00 / 0.00 / 0.00	1.00 / 1.00 / 0.00 / 0.00	1.00 / 1.00 / 0.00 / 0.00
Imagenet	0.85 / 0.78 / 0.25 / 0.20	0.58 / 0.56 / 0.28 / 0.60	0.60 / 0.56 / 0.30 / 0.58	0.62 / 0.59 / 0.32 / 0.50	0.69 / 0.64 / 0.36 / 0.35
LAION	0.85 / 0.75 / 0.32 / 0.17	0.74 / 0.66 / 0.25 / 0.42	0.73 / 0.66 / 0.26 / 0.41	0.73 / 0.66 / 0.30 / 0.38	0.74 / 0.68 / 0.33 / 0.31
LSUN	0.90 / 0.81 / 0.23 / 0.15	0.65 / 0.61 / 0.24 / 0.54	0.66 / 0.61 / 0.29 / 0.49	0.69 / 0.64 / 0.32 / 0.41	0.74 / 0.68 / 0.32 / 0.32
RAISE	0.80 / 0.77 / 0.15 / 0.32	0.83 / 0.76 / 0.03 / 0.46	0.85 / 0.78 / 0.03 / 0.41	0.83 / 0.81 / 0.04 / 0.34	0.81 / 0.82 / 0.04 / 0.31

Table 26. AUC, BA, FPR, and FNR for the JPEG compression scenario for the [82] detector.

	Original format	QF = 65	QF = 75	QF = 85	QF = 95
	AUC / BA / FPR / FNR	AUC / BA / FPR / FNR	AUC / BA / FPR / FNR	AUC / BA / FPR / FNR	AUC / BA / FPR / FNR
Imagenet	0.94 / 0.84 / 0.30 / 0.01	0.52 / 0.50 / 0.01 / 1.00	0.52 / 0.50 / 0.01 / 1.00	0.51 / 0.50 / 0.01 / 0.98	0.51 / 0.53 / 0.08 / 0.86
COCO	0.91 / 0.82 / 0.34 / 0.01	0.42 / 0.50 / 0.00 / 1.00	0.42 / 0.50 / 0.00 / 1.00	0.42 / 0.50 / 0.00 / 1.00	0.42 / 0.49 / 0.05 / 0.96
CelebA	1.00 / 0.99 / 0.01 / 0.00	0.34 / 0.50 / 0.00 / 1.00	0.31 / 0.50 / 0.00 / 1.00	0.32 / 0.50 / 0.00 / 1.00	0.31 / 0.50 / 0.00 / 1.00
LSUN	1.00 / 0.99 / 0.00 / 0.03	0.47 / 0.50 / 0.00 / 1.00	0.48 / 0.50 / 0.00 / 1.00	0.49 / 0.50 / 0.00 / 1.00	0.53 / 0.51 / 0.01 / 0.98
LAION	0.99 / 0.97 / 0.02 / 0.05	0.30 / 0.50 / 0.00 / 0.99	0.31 / 0.50 / 0.00 / 0.99	0.33 / 0.51 / 0.00 / 0.99	0.34 / 0.51 / 0.02 / 0.97

Table 27. BA, FPR, and FNR for the HEIC compression scenario for the [82] detector.

	Original format	QF = 65	QF = 75	QF = 85	QF = 95
	BA / FPR / FNR	BA / FPR / FNR	BA / FPR / FNR	BA / FPR / FNR	BA / FPR / FNR
Imagenet	0.84 / 0.30 / 0.01	0.50 / 0.00 / 1.00	0.50 / 0.00 / 1.00	0.50 / 0.00 / 1.00	0.50 / 0.00 / 1.00
COCO	0.82 / 0.34 / 0.01	0.50 / 0.00 / 1.00	0.50 / 0.00 / 1.00	0.50 / 0.00 / 1.00	0.50 / 0.00 / 1.00
CelebA	0.99 / 0.01 / 0.00	0.50 / 0.00 / 1.00	0.50 / 0.00 / 1.00	0.50 / 0.00 / 1.00	0.50 / 0.00 / 1.00
LSUN	0.99 / 0.00 / 0.03	0.51 / 0.00 / 0.98	0.52 / 0.00 / 0.95	0.55 / 0.00 / 0.91	0.56 / 0.00 / 0.88
LAION	0.97 / 0.02 / 0.05	0.50 / 0.00 / 1.00	0.50 / 0.00 / 1.00	0.50 / 0.00 / 1.00	0.50 / 0.00 / 1.00
Average	0.92 / 0.13 / 0.02	0.50 / 0.00 / 1.00	0.50 / 0.00 / 0.99	0.51 / 0.00 / 0.98	0.51 / 0.00 / 0.97

Table 28. BA, FPR, and FNR for the WebP compression scenario for the [82] detector.

	Original format	QF = 65	QF = 75	QF = 85	QF = 95
	BA / FPR / FNR	BA / FPR / FNR	BA / FPR / FNR	BA / FPR / FNR	BA / FPR / FNR
Imagenet	0.84 / 0.30 / 0.01	0.50 / 0.00 / 1.00	0.50 / 0.01 / 1.00	0.52 / 0.04 / 0.92	0.54 / 0.13 / 0.79
COCO	0.82 / 0.34 / 0.01	0.50 / 0.00 / 1.00	0.50 / 0.00 / 1.00	0.50 / 0.02 / 0.98	0.49 / 0.11 / 0.91
CelebA	0.99 / 0.01 / 0.00	0.50 / 0.00 / 1.00	0.50 / 0.00 / 1.00	0.50 / 0.00 / 1.00	0.50 / 0.00 / 1.00
LSUN	0.99 / 0.00 / 0.03	0.50 / 0.00 / 1.00	0.50 / 0.00 / 1.00	0.50 / 0.00 / 1.00	0.53 / 0.01 / 0.94
LAION	0.97 / 0.02 / 0.05	0.50 / 0.00 / 0.99	0.50 / 0.00 / 0.99	0.51 / 0.00 / 0.98	0.52 / 0.01 / 0.95
Average	0.92 / 0.13 / 0.02	0.50 / 0.00 / 1.00	0.50 / 0.00 / 1.00	0.51 / 0.01 / 0.98	0.51 / 0.05 / 0.92

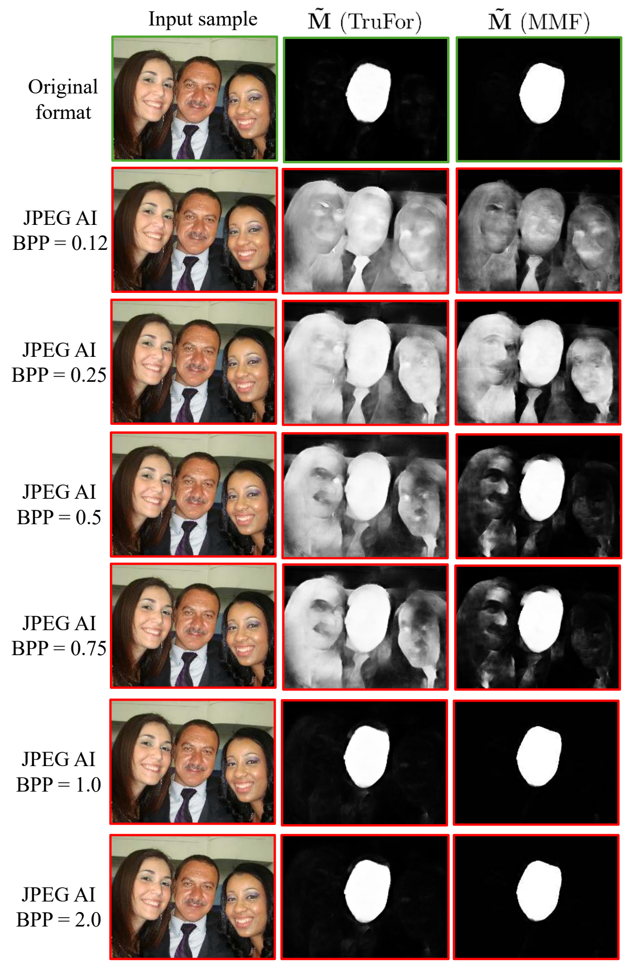

Figure 14. Output of the considered detectors for the same DS01 input under different JPEG AI compression settings.

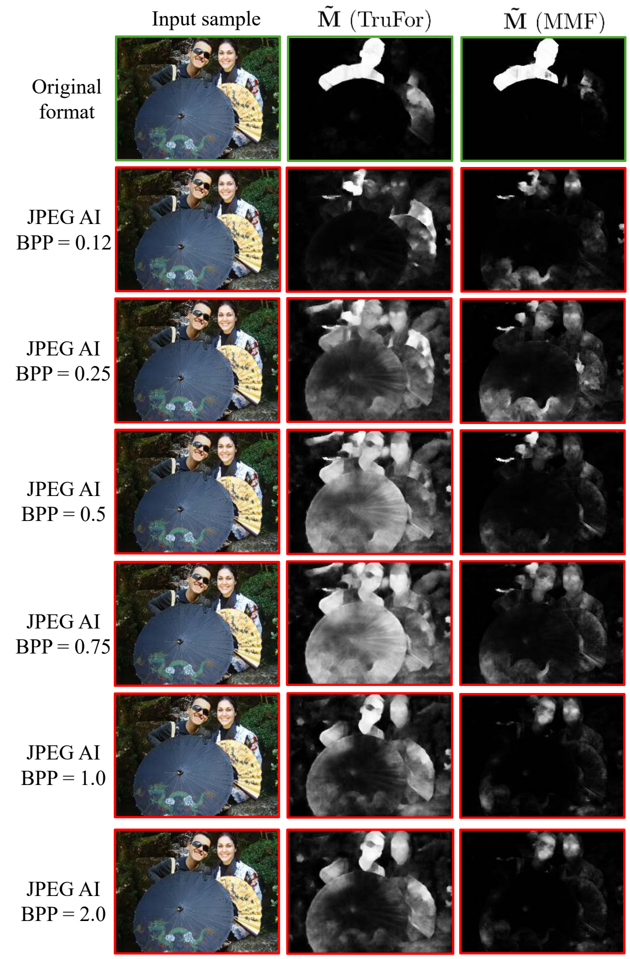

Figure 15. Output of the considered detectors for the same DS01 input under different JPEG AI compression settings.

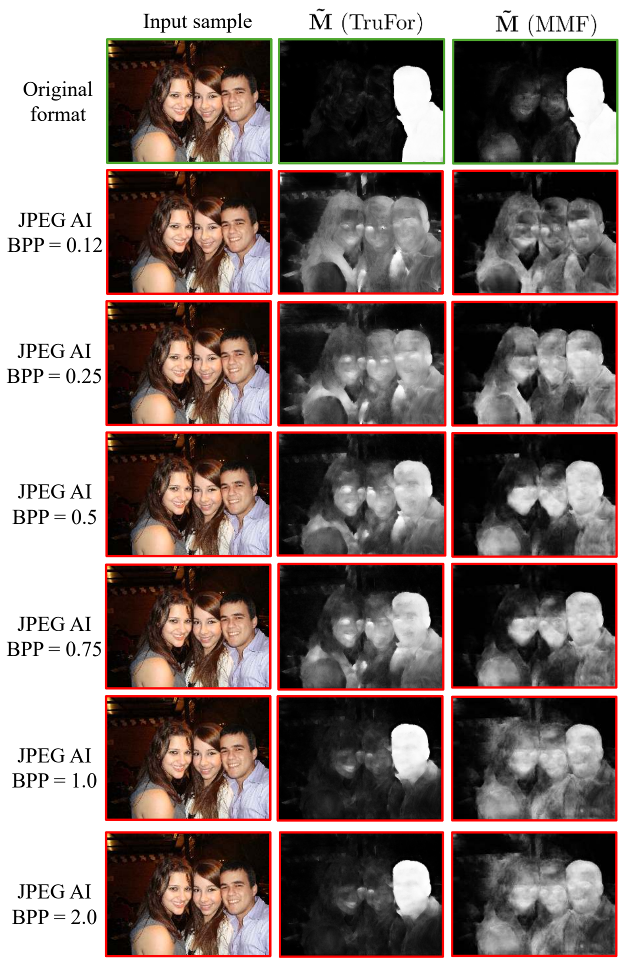

Figure 16. Output of the considered detectors for the same DS01 input under different JPEG AI compression settings.

Figure 17. Output of the considered detectors for the same DS01 input under different JPEG AI compression settings.

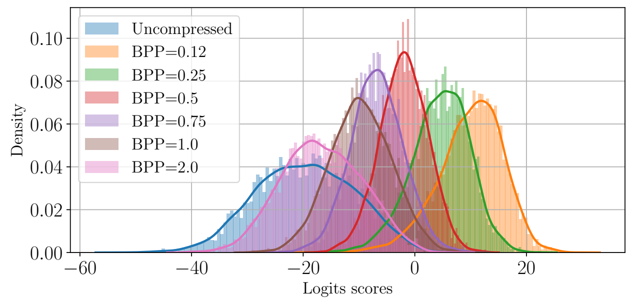

(a) Single JPEG AI compression.

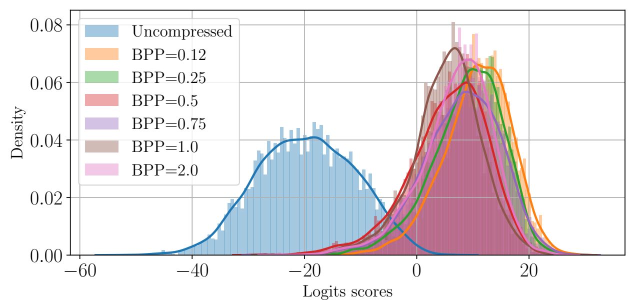

(b) Double JPEG AI compression, starting BPP= 0.12.

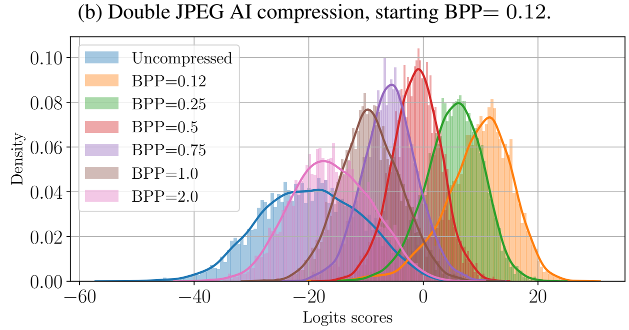

(c) Double JPEG AI compression, starting BPP= 2.0.

Figure 18. Scores distribution over COCO pristine samples of the [43] detector considering different JPEG AI compression stages.

Figure 19. Output of MMFusion for DSO-1 double JPEG AI compressed images. The second compression stage is executed with BPP equal to 0.12. The first compression stage BPP value varies from 0.12 to 2.0 from top to bottom.

Figure 20. Output of MMFusion for DSO-1 double JPEG AI compressed images. The second compression stage is executed with BPP equal to 2.0. The first compression stage BPP value varies from 0.12 to 2.0 from top to bottom.